Article

Cell Reports

PPARγ Interaction with UBR5/ATMIN Promotes DNA Repair to Maintain Endothelial Homeostasis

Graphical Abstract

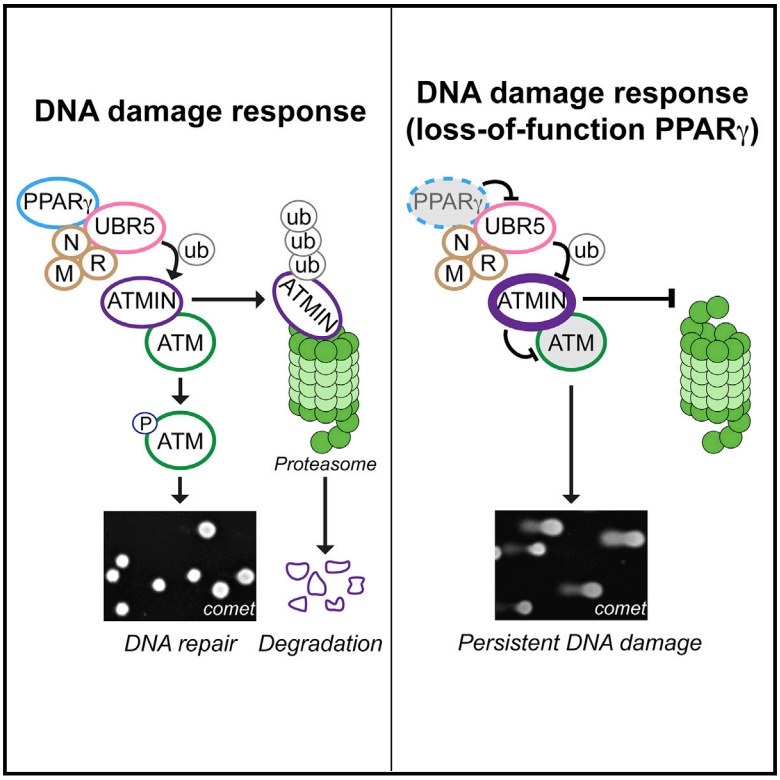

Highlights

- PPARγ proteomics identifies interactions with the MRE11-RAD50-NBS1 complex and UBR5
- Upon DNA damage, PPARγ promotes UBR5-mediated ATMIN degradation to activate ATM
- PPARγ-UBR5 interaction is disrupted in endothelial cells isolated from PAH patients
- Depleting ATMIN in PAH endothelial cells restores ATM signaling upon DNA damage

Authors

Caiyun G. Li, Cathal Mahon, Nathaly M. Sweeney, ..., Mark Kaschwich, Karlene A. Cimprich, Marlene Rabinovitch

Correspondence

marlener@stanford.edu

In Brief

Li et al. identify PPARγ interactions with MRN and UBR5. PPARγ promotes UBR5-mediated ATMIN degradation, necessary for ATM activation upon DNA damage. Pulmonary arterial hypertension (PAH) endothelial cells exhibit genomic instability and disrupted PPARγ-UBR5 interaction. Blocking ATMIN restores ATM signaling in these cells, highlighting the significance of the PPARγ-ATMIN axis.

Li et al., 2019, Cell Reports *26*, 1333–1343
January 29, 2019
https://doi.org/10.1016/j.celrep.2019.01.013

CellPress

Cell Reports
Article

PPARγ Interaction with UBR5/ATMIN Promotes DNA Repair to Maintain Endothelial Homeostasis

Caiyun G. Li,[1] Cathal Mahon,[2,3] Nathaly M. Sweeney,[1,7] Erik Verschueren,[2] Vivek Kantamani,[1] Dan Li,[1] Jan K. Hennigs,[1] David P. Marciano,[4] Isabel Diebold,[1] Ossama Abu-Halawa,[1] Matthew Elliott,[1] Silin Sa,[1] Feng Guo,[5] Lingli Wang,[1] Aiqin Cao,[1] Christophe Guignabert,[1] Julie Sollier,[6] Nils P. Nickel,[1] Mark Kaschwich,[1] Karlene A. Cimprich,[6] and Marlene Rabinovitch[1,8,*]

[1]The Vera Moulton Wall Center for Pulmonary Vascular Disease, Department of Pediatrics and Cardiovascular Institute, Stanford School of Medicine, Stanford, CA 94305, USA
[2]California Institute for Quantitative Biosciences, Department of Cellular and Molecular Pharmacology, University of California-San Francisco, San Francisco, CA 94158, USA
[3]Department of Pharmaceutical Chemistry, University of California-San Francisco, San Francisco, CA 94158, USA
[4]Department of Genetics, Stanford School of Medicine, Stanford, CA 94305, USA
[5]Department of Medicine, Stanford School of Medicine, Stanford, CA 94305, USA
[6]Department of Chemical and Systems Biology, Stanford School of Medicine, Stanford, CA 94305, USA
[7]Present address: Department of Pediatrics University of California-San Diego, San Diego, CA 92103, USA
[8]Lead Contact
*Correspondence: marlener@stanford.edu
https://doi.org/10.1016/j.celrep.2019.01.013

SUMMARY

Using proteomic approaches, we uncovered a DNA damage response (DDR) function for peroxisome proliferator activated receptor γ (PPARγ) through its interaction with the DNA damage sensor MRE11-RAD50-NBS1 (MRN) and the E3 ubiquitin ligase UBR5. We show that PPARγ promotes ATM signaling and is essential for UBR5 activity targeting ATM interactor (ATMIN). PPARγ depletion increases ATMIN protein independent of transcription and suppresses DDR-induced ATM signaling. Blocking ATMIN in this context restores ATM activation and DNA repair. We illustrate the physiological relevance of PPARγ DDR functions by using pulmonary arterial hypertension (PAH) as a model that has impaired PPARγ signaling related to endothelial cell (EC) dysfunction and unresolved DNA damage. In pulmonary arterial ECs (PAECs) from PAH patients, we observed disrupted PPARγ-UBR5 interaction, heightened ATMIN expression, and DNA lesions. Blocking ATMIN in PAH PAEC restores ATM activation. Thus, impaired PPARγ DDR functions may explain the genomic instability and loss of endothelial homeostasis in PAH.

INTRODUCTION

Peroxisome proliferator activated receptor γ (PPARγ) is a member of the nuclear receptor family that interacts with canonical retinoic acid receptors (RXR) (Chandra et al., 2008) and other co-factors as a transcription factor complex in multiple cell types, including vascular cells (Alastalo et al., 2011). Aberrant PPARγ-mediated transcription has been implicated in disease conditions, including obesity, diabetes, cancer, inflammation, and vascular disorders (Ahmadian et al., 2013; Rabinovitch, 2010) that include atherosclerosis (Duval et al., 2002), aortic aneurysm (Hamblin et al., 2010), and pulmonary arterial hypertension (PAH) (Rabinovitch, 2010). Endothelial dysfunction is a feature of all these vascular diseases, and in PAH, it is associated with the obliteration and loss of microvessels that increase resistance to pulmonary blood flow and can culminate in heart failure and the need for a lung transplant (Rabinovitch, 2012).

Mice with PPARγ deleted in endothelial cells (ECs) (*Tie2-Pparγ*$^{-/-}$) develop pulmonary hypertension that persists upon re-exposure to room air after hypoxia (Guignabert et al., 2009). In human pulmonary arterial ECs (PAECs), an interaction between PPARγ and β-catenin co-regulates the gene expression of apelin, a major factor that promotes PAEC survival and suppresses smooth muscle cell proliferation (Alastalo et al., 2011). This interaction is disrupted by rosiglitazone, an agonist previously used to treat type II diabetes (Alastalo et al., 2011). These observations reinforce the need to discover interactions between PPARγ and other proteins that are perturbed in PAH and other vascular disorders and have pharmacologic relevance.

Here, we report the results of a proteomic approach using affinity purification with mass spectrometry (AP-MS) to identify PPARγ nuclear interacting proteins. These studies uncovered PPARγ interactions with the DNA damage sensor MRN (MRE11-RAD50-NBS1) and the E3 ubiquitin ligase UBR5 and a role for PPARγ in the DNA damage response (DDR) pathway. We showed that PPARγ promotes UBR5 ubiquitin ligase activity and regulates ATM interactor (ATMIN) levels, thereby permitting efficient ATM phosphorylation and the initiation of DNA repair upon DNA damage. Perturbation of this axis is observed in PAH and can account for unresolved DNA damage that is associated with impaired endothelial functions (de Jesus Perez et al., 2014; Diebold et al., 2015).

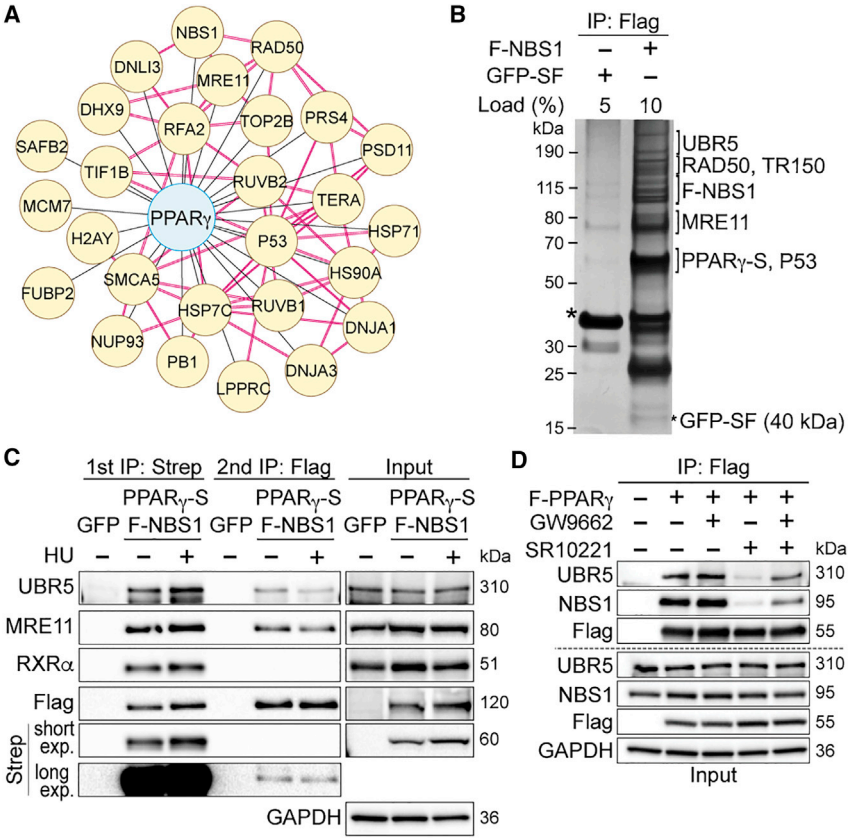

Figure 1. PPARγ Interacts with the MRE11-RAD50-NBS1 (MRN) Complex and UBR5 in 293T Cells

(A) A network of PPARγ and its interactors (yellow) in the DNA damage response (DDR) and DNA replication pathway. Red connections denote interactions obtained from the protein complex enrichment analysis tool (COMPLEAT) database.

(B) Silver staining shows gel fragments containing proteins (identified by MS) sequentially co-purified with tagged PPARγ (-2xStrep, S) and NBS1 (-FLAG, F) but not with green fluorescent protein (GFP-SF).

(C) Representative immunoblots of interactions between the PPARγ-NBS1 complex with RXRα and UBR5 upon hydroxyurea (HU) treatment (24 h).

(D) The 293T cells expressing FLAG-PPARγ were pretreated with GW9662 (5 μM, 1 h) and treated with SR10221 (5 μM, 24 h) (GW+SR). Controls included are cells treated with DMSO (vehicle), GW9662, or SR10221 only. Cells expressing FLAG-vector were used as the immunoprecipitation negative control. Representative immunoblots show effects of GW9662 pretreatment together with SR10221 on interactions between PPARγ and UBR5/NBS1.

See also Figures S1 and S2 and Tables S1–S4.

RESULTS

AP-MS Identified PPARγ Interactions with MRN and UBR5 Independent of RXRα

We transiently transfected 293T cells with a FLAG-tagged PPARγ1 construct and isolated nuclear extracts in the presence of micrococcal nuclease for affinity purification using a FLAG antibody. We used 293T cells for their high transfection efficiency that permitted efficient pull-down of FLAG-PPARγ and detection of interactors. The quadruplicate AP-MS screen revealed 352 proteins that co-purified with FLAG-PPARγ with a $\log_2$ fold change (Log_2FC) of >1.5 and an adjusted p value (adj. P) $\leq$ 0.05 (Figure S1A). Not surprisingly, we detected known PPARγ interactors, such as mediator of RNA polymerase II transcription subunit 1 and 24 (MED1 and MED24, respectively), promyelocytic leukemia protein (PML), p53, and others. We ranked 87 proteins as high-confidence PPARγ-interacting proteins, and those included the canonical partners RXRα and β (Figure S1A; Table S1). Using databases of published physical and functional interactions, we constructed and analyzed networks of high confidence proteins for enriched biological functions. In addition to cellular metabolism, we observed DDR and DNA replication among the most enriched functions (Figure 1A; Table S2). From the DDR network, four interactions were verified by co-immunoprecipitation, i.e., the components of the DNA damage sensing complex MRN (MRE11-RAD50-NBS1) and p53 (Figure S1B).

MRN initiates the DDR pathway using NBS1 to recruit proteins necessary for DNA repair (Reinhardt and Yaffe, 2013). We hypothesize that PPARγ binds to MRN via NBS1. To test this, we used tandem affinity purification (TAP) of PPARγ-2x Streptavidin (PPARγ-2xStrep) and FLAG-NBS1 in 293T cells, and the crosslinking agent bis(sulfosuccinimidyl)suberate (BS3) was added on beads before elution. The crosslinked immunocomplexes were analyzed by mass spectrometry (XL-MS) (Figure S1C). XL-MS identified three PPARγ peptides crosslinked to NBS1 (Figure S1D), demonstrating a direct interaction. Using structural mapping based on PPARγ crystal structure (Chandra et al., 2008), we located two of the three peptides in the zinc-finger motif within the PPARγ DNA-binding domain (DBD) and one in the ligand-binding domain (LBD) (Figures S1E and S1F). These data suggest that NBS1 binding might interfere with PPARγ transcription factor function. We used size-exclusion chromatography of nuclear extracts overexpressing PPARγ-2xStrep and FLAG-NBS1 and showed that PPARγ exists in multiple pools: a higher molecular weight (MW, approximated >1,500 kDa) pool, a lower MW (approximated 67–440 kDa) pool, and a monomeric pool (from overexpression, <67 kDa). NBS1 and RXRα reside in the high and low MW PPARγ pools, respectively, supporting mutually exclusive PPARγ interactions with NBS1 or RXRα (Figure S2A). In the absence of NBS1, we also found that *PPARγ* and three out of the seven PPARγ target genes were upregulated (Figure S2B). The requirement of PPARγ-LBD for MRN interactions was confirmed using mutagenesis (Figure S2C). These data suggest that upon MRN binding, PPARγ undergoes structural changes, which can interfere with its transcription factor property, implicating an independent function for PPARγ.

To investigate PPARγ functions in relation to MRN binding, we performed initial silver staining of the TAP elution from unperturbed cell lysates and identified all components of MRN but not RXRα (Figure 1B), supporting our XL-MS and size-exclusion chromatography results. Silver-stained gel fragments from the TAP elution also identified TR150 (thyroid hormone receptor-associated protein 3, encoded by *THRAP3*) and the ubiquitin ligase UBR5 co-purifying with the PPARγ-MRN complex (Figure 1B). Under conditions of DNA damage induced by hydroxyurea (HU), TAP-MS revealed associations of UBR5 and TR150 with the PPARγ-MRN complex (Figure 1C; Tables S3 and S4). We performed nuclear co-immunoprecipitation (co-IP) of endogenous UBR5 and NBS1 and showed that both UBR5 and NBS1 bind strongly to PPARγ but weakly to each other (Figure S2D). This was confirmed by co-IP of UBR5 and PPARγ in the absence of NBS1 (Figure S2E). To verify the specificity of these PPARγ interactions, we altered PPARγ conformations by using the pharmacological modulator SR10221, which destabilizes helix 12 in the PPARγ LBD (Marciano et al., 2015). SR10221 disrupted PPARγ interactions with MRN and UBR5, which were restored by pre-treatment with GW9662, which blocks the SR10221 target site (Figure 1D). Our proteomic and biochemical data suggest that PPARγ interactions with MRN and UBR5 implicate a potential role for PPARγ in the DDR pathway.

PPARγ Promotes the Initiation of ATM Signaling

The MRN complex (Lee and Paull, 2004) and UBR5 (Zhang et al., 2014) are required for ATM activity, which is necessary for DNA repair induced by genotoxic agents. In this study, we activated ATM signaling using doxorubicin (DoxR), which intercalates DNA and generates double-strand breaks (Kurz et al., 2004), and HU, which induces replication fork collapse and a progressive accumulation of double-strand breaks (Cuadrado et al., 2006). We first verified endogenous nuclear PPARγ interactions with UBR5 and MRN at baseline and in response to DoxR or HU (Figure 2A). To determine if PPARγ is necessary for ATM activation, we depleted PPARγ using small interfering RNA (siRNA) and induced damage using HU and DoxR. The loss of PPARγ and UBR5 reduced HU-mediated ATM phosphorylation (pATM, Ser1981) and its targets KAP1 (Ser824) (Ziv et al., 2006), γH2AX (Ser139) (Burma et al., 2001), and SMC1 (Ser966) (Yazdi et al., 2002) (which was not affected by siUBR5) (Figure 2B; densitometry in Figure S3A). PPARγ/UBR5-dependent ATM signaling was also evident in response to DoxR treatment (Figure S3B). We further investigated the role of PPARγ in HU-induced DNA damage because replication stress damage is relevant to PAH (de Jesus Perez et al., 2014).

PPARγ and UBR5 Modulate ATMIN Protein Levels through Ubiquitination

To understand how PPARγ and UBR5 regulate ATM signaling, we determined whether PPARγ is required for UBR5 E3 ubiquitin ligase activity. Indeed, PPARγ depletion inhibited UBR5-mediated ubiquitination, judging by a decrease in ubiquitinated proteins immunoprecipitated with UBR5 (Figure 2C). We further investigated whether PPARγ depletion affects ATMIN levels, an UBR5 substrate that regulates ATM phosphorylation. Previous studies indicated that UBR5 ubiquitinates ATMIN upon ionizing radiation to release and allow ATM activation (Zhang et al., 2014; Zhang et al., 2012). In contrast, other studies have shown the opposite with replication stress, i.e., that loss of ATMIN suppresses ATM activation (Schmidt et al., 2014).

Here, we observed that upon depletion of PPARγ or UBR5, ATMIN levels were elevated both at baseline and in response to HU in association with the suppression of the ATM target pRPA2 (Ser4/8) (Liu et al., 2012) (Figures 2D and 2E; densitometry in Figures S3C and S3D). Consistent with the function for PPARγ related to UBR5 ubiquitin ligase activity, elevated ATMIN protein in the absence of PPARγ or UBR5 was accompanied by a decrease in its ubiquitination (Figure 2F). Moreover, ubiquitination of ATMIN was associated with its degradation since the proteasome inhibitor MG132 maintains ATMIN protein levels (Figure 2F, input panel). In the absence of UBR5, PPARγ remained bound to the truncated FLAG-ATMIN (aa1-354), supporting UBR5 as downstream of PPARγ in ATMIN regulation (Figure S3E). In addition, both UBR5 and PPARγ bind to FLAG-ATMIN with and without HU, with UBR5 binding more sustained upon HU treatment (Figure S3F). The effects of PPARγ depletion on protein degradation was further evident judging by the reduced cellular lysine (K)48-linked ubiquitins, which represent protein degradative signals (Glickman and Ciechanover, 2002). This reduction was restored by overexpressing siRNA-resistant PPARγ (siResPPARγ) (Figure S3G). Since PPARγ is a transcription factor, we confirmed that ATMIN mRNA levels were not significantly altered by the depletion of PPARγ or of UBR5 (Figure 2G). Taken together, our data indicate that the loss of PPARγ alters cellular protein degradative signals and, specifically, it increases ATMIN levels by suppressing UBR5-mediated ubiquitination, and that this function is not related to PPARγ-mediated transcription.

PPARγ-DDR Function Is Conserved in ECs

We and others showed that PPARγ promotes endothelial survival and regeneration (Alastalo et al., 2011; Vattulainen-Collanus et al., 2016). In a transgenic mouse with deficient endothelial PPARγ, pulmonary hypertension and adverse vascular remodeling did not reverse following re-exposure to room air after chronic hypoxia (Guignabert et al., 2009). As impaired PPARγ function and chromosomal instability related to persistent DNA damage are features of PAECs from patients with PAH (Aldred et al., 2010), we determined if PPARγ functions in DDR are compromised in PAH and could contribute to the loss of vascular homeostasis.

We first verified nuclear PPARγ and UBR5 interactions in primary human PAECs (Figure 3A). Consistent with our findings in 293T cells, PPARγ depletion in PAECs also led to reduced pATM, pRPA2, and γH2AX upon prolonged HU treatment (Figure 3B; densitometry, Figures S4A and S4B). To confirm the specificity of PPARγ-ATM signaling, we restored pATM in human umbilical venous ECs (HUVECs) by overexpressing siResPPARγ (Figure 3C; densitometry, Figure S4C). HUVECs were used to withstand the cytotoxicity from DNA and siRNA sequential transfections. Verifying ATMIN regulation of PPARγ-dependent ATM signaling in ECs, we depleted ATMIN in addition to PPARγ and observed that this restored pATM and its target pKAP1 (Figure 3D; densitometry, Figure S4D). Although ATMIN regulation of ATM signaling is highly context dependent

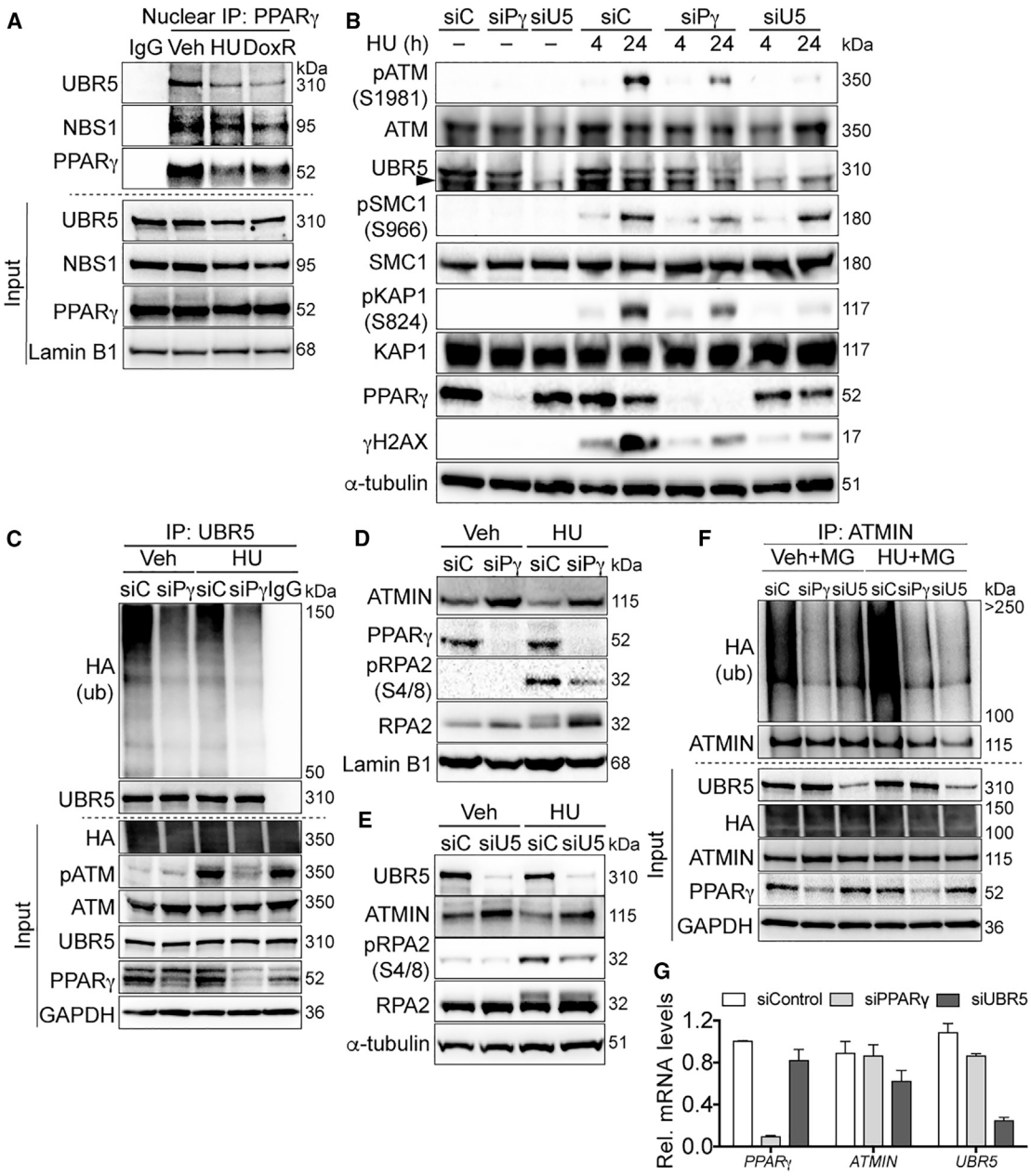

Figure 2. PPARγ Promotes ATM Signaling by Increasing UBR5-Mediated ATMIN Ubiquitination in 293T Cells

(A) Representative immunoblots of endogenous nuclear PPARγ interactions with MRN and UBR5 at baseline and upon DNA damage induced by HU and doxorubicin (DoxR).

(B) Representative immunoblots of HU-induced pATM and its targets with PPARγ or UBR5 depletion.

(C) Representative immunoblots of reduced UBR5 binding to ubiquitinated proteins with PPARγ depletion.

(D and E) Representative immunoblots of ATMIN and pRPA2 levels with PPARγ (D) or UBR5 (E) depletion upon HU treatments.

(F) Cells were transfected with HA-tagged ubiquitin and subsequently the siRNA as indicated. Cells were treated with the proteasome inhibitor MG132 (MG) for 2 h before lysis in a denaturing buffer. Endogenous ATMIN was immunoprecipitated to determine its polyubiquitinated form. Representative immunoblots show effects of PPARγ or UBR5 depletion on endogenous ATMIN ubiquitination detected by anti-hemagglutinin (HA) antibody.

(G) Quantitative real-time PCR shows effects of PPARγ or UBR5 depletion by the respective siRNA on *ATMIN* mRNA levels (normalized to β-actin mRNA).

siC, siControl; siPγ, siPPARγ; siU5, siUBR5; Veh; vehicle. Error bars, mean ± SEM.

See also Figure S3.

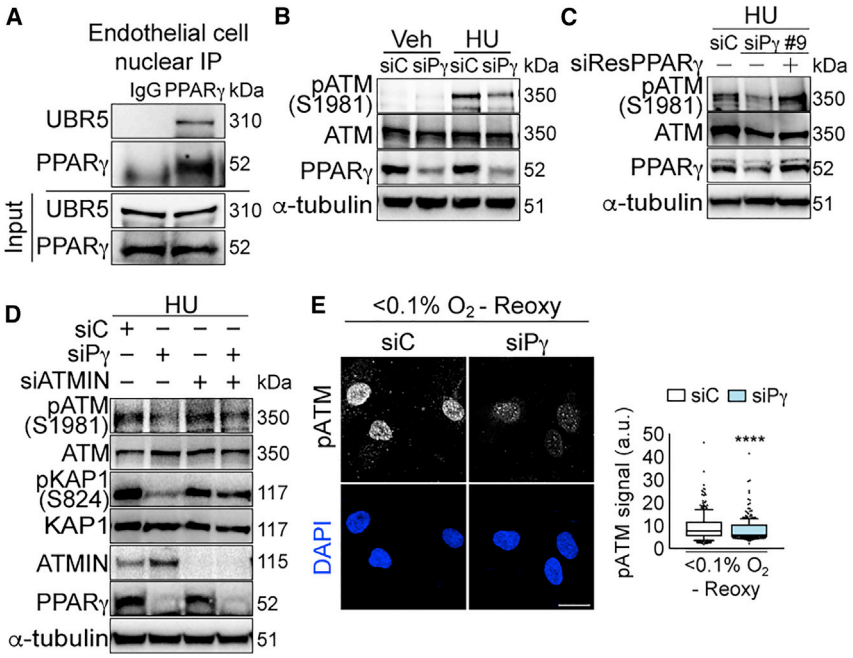

Figure 3. PPARγ-ATMIN Regulation of ATM Signaling Is Conserved in Primary Human Endothelial Cells

(A) Representative immunoblots of endogenous nuclear PPARγ interaction with UBR5 in primary pulmonary arterial endothelial cells (PAECs) isolated from controls (Table S5).

(B) Representative immunoblots of HU-induced pATM expression with PPARγ depletion in PAECs.

(C) Representative immunoblots of restoration of HU-induced pATM expression with siRNA (siPPARγ#9)-resistant PPARγ overexpression in human umbilical venous ECs (HUVECs).

(D) Representative immunoblots of HU-induced pATM and pKAP1 with PPARγ or/and ATMIN depletions in PAECs.

(E) Confocal microscopy of PAECs shows effects of PPARγ depletion on pATM foci with hypoxia (<0.1% O_2, 24 h) and reoxygenation (10 min). The line in the box of the box and whisker plots marks the median and whiskers correspond to the 10th to 90th percentiles. Unpaired Student t test was used. ****p < 0.0001. Scale bars, 20 μm.

siC, siControl; siPγ, siPPARγ. See also Figure S4.

(Leszczynska et al., 2016; Schmidt et al., 2014; Zhang et al., 2014), our results demonstrate that in the absence of PPARγ, abnormal accumulation of ATMIN suppresses ATM activation in response to DNA damage.

We also verified the inhibitory effects of siPPARγ on pATM and γH2AX foci by using immunofluorescence in PAEC (Figures S4E and S4F). This response was replicated with three individual siRNAs targeting PPARγ (Figure S4G). Importantly, the reduced ATM signaling upon PPARγ depletion was not due to altered cell cycle progression (Figure S4H). Since elevated oxidative stress has been implicated in PAH pathogenesis (Diebold et al., 2015) and ATM signaling is activated by oxidative stress (Hammond et al., 2003), we investigated if PPARγ also promotes ATM signaling upon oxidant injury. By exposing PAECs to hypoxia (<0.1% O_2, 24 h) and reoxygenation (10 min), we detected the presence of 8-oxo-2′-deoxyguanosine (8-oxo-dG) foci (S4I), a marker for oxidative damage DNA (Cheng et al., 1992). We showed that PPARγ depletion also suppressed oxidative stress-induced pATM (Figure 3E; replicates, Figure S4J).

The PPARγ-ATMIN Axis Is Required for Endothelial DNA Repair and Homeostasis

We now showed that PPARγ is necessary to initiate the DDR, and we hypothesize that it is also important for DNA repair. We used the comet assay and demonstrated that PPARγ depletion did not affect the magnitude of DNA damage, as judged by comet tails assessed after a 6-h exposure to HU (Figure 4A; replicates, Figure S5A), but the capacity to repair DNA was reduced, as judged by persistent comet tails after a 24-h recovery period. We also examined levels of pRPA2 and γH2AX damage foci during recovery (24–72 h), as evidence of unrepaired DNA lesions. These foci were resolved in the control cells but were sustained in PPARγ-depleted PAECs (Figure 4B; replicates, Figure S5B). We validated that ATMIN also functions in PPARγ-dependent DNA repair by demonstrating that depletion of ATMIN in addition to PPARγ resolved pRPA2 foci during recovery (Figures 4C and 4D; densitometry and replicates, Figures S5C and S5D).

We then determined whether unresolved DNA damage accompanied the pulmonary hypertension that did not reverse in mice with PPARγ depleted in ECs (*Tie2-Pparγ*$^{-/-}$) that were re-exposed to room air after chronic hypoxia (Guignabert et al., 2009). Lung sections from *Tie2-Pparγ*$^{-/-}$ mice and wild-type littermates were co-stained with von Willebrand factor (vWF) antibody to detect ECs and γH2AX antibody. Confocal microscopy revealed increased γH2AX in the ECs of the mutant versus control mice previously studied following re-exposure to room air (Figure 4E). These data further supported our mechanistic studies in cultured PAECs that link PPARγ to regulation of DNA damage sensing and repair.

Reduced PPARγ-UBR5 Interaction, Elevated ATMIN, and Impaired DDR in PAH-PAEC

The loss of genome integrity and an increased propensity for apoptosis and transformation are key features of PAECs from PAH patients (PAH-PAECs) (Aldred et al., 2010; Hopper et al., 2016; Ranchoux et al., 2015; Sa et al., 2016). We, therefore, assessed evidence of unrepaired DNA damage in PAH versus unused donor control lung sections and in cultured PAECs harvested from explanted PAH lungs and from control lungs. Demographic information related to controls (unused donor) and PAH-PAECs is provided in Table S5. Representative cell images indicating healthy, actively proliferating primary PAEC cultures are shown in Figure S6A.

Increased γH2AX foci were evident in PAH versus control PAECs in lung tissue sections (Figure 5A), and in cell cultures, there were more extended comet tails (Figure 5B) in PAH-PAECs

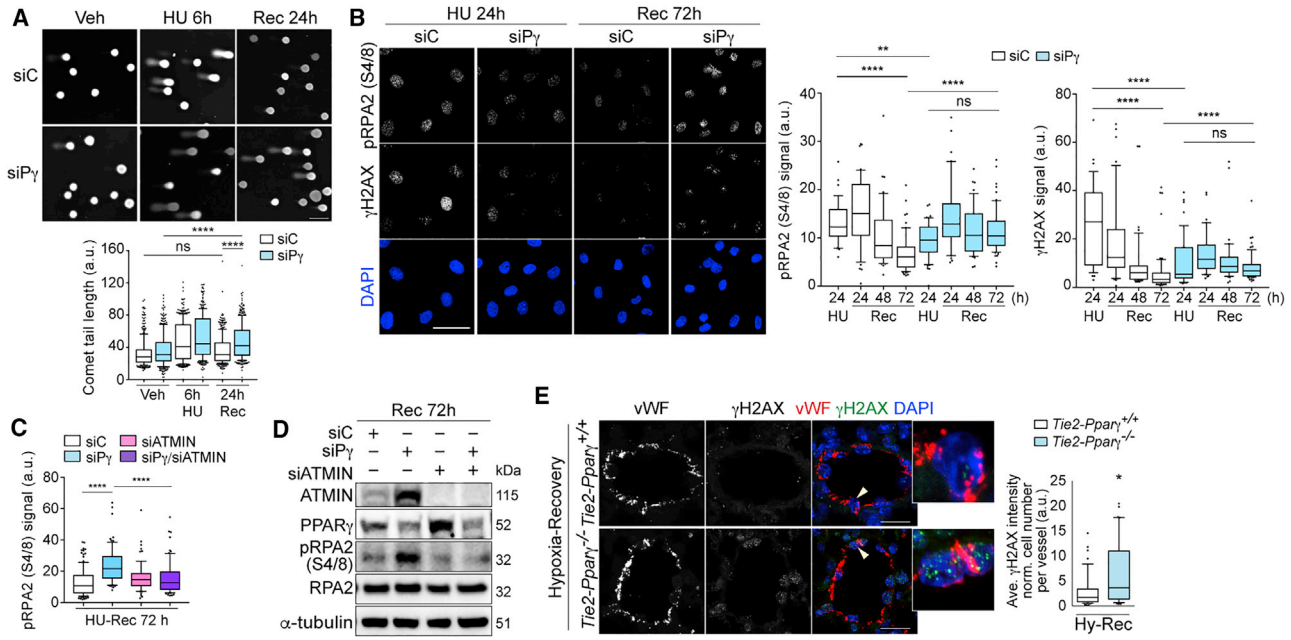

Figure 4. PPARγ Promotes DNA Repair through ATMIN in Primary Human ECs

(A) Comet assay shows effects of PPARγ depletion on comet tail lengths after 24-h recovery (Rec 24h) from 6 h of HU (HU 6h) treatment.

(B) Confocal microscopy shows effects of PPARγ depletion on unresolved γH2AX and pRPA2 foci over 72 h after recovery (Rec 72h) from 24 h of HU (HU 24h) treatment. Recovery time points are as indicated.

(C) Quantification of pRPA2 foci with PPARγ or/and ATMIN depletion. Cells were fixed and analyzed using confocal microscopy at 72 h after recovery from 24 h of HU treatment.

(D) Representative immunoblots of ATMIN and pRPA2 levels from the same experimental as in (C).

(E) Confocal microscopy shows staining of γH2AX foci in pulmonary ECs (labeled by vWF) in *Tie2-Pparγ*$^{-/-}$ mice and wild-type littermates subjected to three weeks of hypoxia (Hy) (10% O_2) and four weeks of recovery in room air (n = 5). Arrowheads indicate cells in insets.

siC, siControl; siPγ, siPPARγ. The line in the box of the box and whisker plots marks the median and whiskers correspond to the 10th to 90th percentiles (A, B, C, and E). Kruskal-Wallis ANOVA test with Dunn's test (A–C). Two-tailed Mann-Whitney test (E). *p < 0.05; **p < 0.01; ****p < 0.0001, ns., not significant. Scale bars, 50 μm (A and B); 20 μm (E). See also Figure S5.

compared with control-PAECs. Upon HU treatment, PAH-PAECs showed reduced pATM foci compared with control-PAECs (Figure 5C; replicates, Figure S6B).

Impaired ATM signaling in PAH-PAECs suggested that the PPARγ-UBR5-ATMIN axis may be dysfunctional in these cells. Indeed, reduced interactions between PPARγ and UBR5 in PAH-PAECs were evident when compared to control-PAECs (Figure 5D). This was independent of PPARγ levels that were similar in controls and PAH-PAECs (Figure 5D, input panel). A possible explanation could be PPARγ or UBR5 post-translational modifications (PTMs), which can confer structural changes that alter protein-protein interactions (Choi et al., 2014a). Consistent with the disruption of the PPARγ-UBR5 complex related to UBR5 ubiquitin ligase activity, we found heightened ATMIN expression in PAH versus control PAECs (Figure 5E; densitometry, Figure S6C). We confirmed that reducing ATMIN levels in PAH-PAECs restored HU-induced pATM foci formation to a level comparable to control-PAECs (Figure 5F; replicates, Figure S6D).

DISCUSSION

Our data obtained from cultured cells, transgenic mice, and clinical samples reveal a non-canonical role for PPARγ in the DDR and, subsequently, in DNA repair. Through its interactions with MRN and UBR5 independent of RXRα, PPARγ promotes ATM signaling in response to genotoxic stimuli. We propose a model in Figure 6, suggesting that the PPARγ DDR complex regulates the ATMIN-ATM interaction necessary for the activation of ATM in response to DNA damage. We provide data showing that PPARγ interaction with UBR5 is required for UBR5-mediated ubiquitination of multiple substrates, including ATMIN. A disrupted PPARγ-UBR5 complex in PAECs from PAH patients results in elevated ATMIN, impaired ATM signaling, and persistent DNA damage. Under these circumstances, reducing ATMIN can restore the DDR and result in efficient DNA repair.

There is much known about PPARγ function related to its transcriptional targets associated with adipocyte differentiation and lipid metabolism and their perturbation in obesity and diabetes (Ahmadian et al., 2013). Our previous work showing differences in the response to PPARγ agonists in endothelial (Alastalo et al., 2011) and smooth muscle cells (Hansmann et al., 2008) led to a more comprehensive investigation of proteins interacting with PPARγ. Using an unbiased proteomic approach in 293T cells, we detected RXRα and RXRβ but not other known PPARγ transcriptional co-factors, such as the nuclear receptor coactivators and corepressors (NCOAs and NCORs) (Koppen and Kalkhoven,

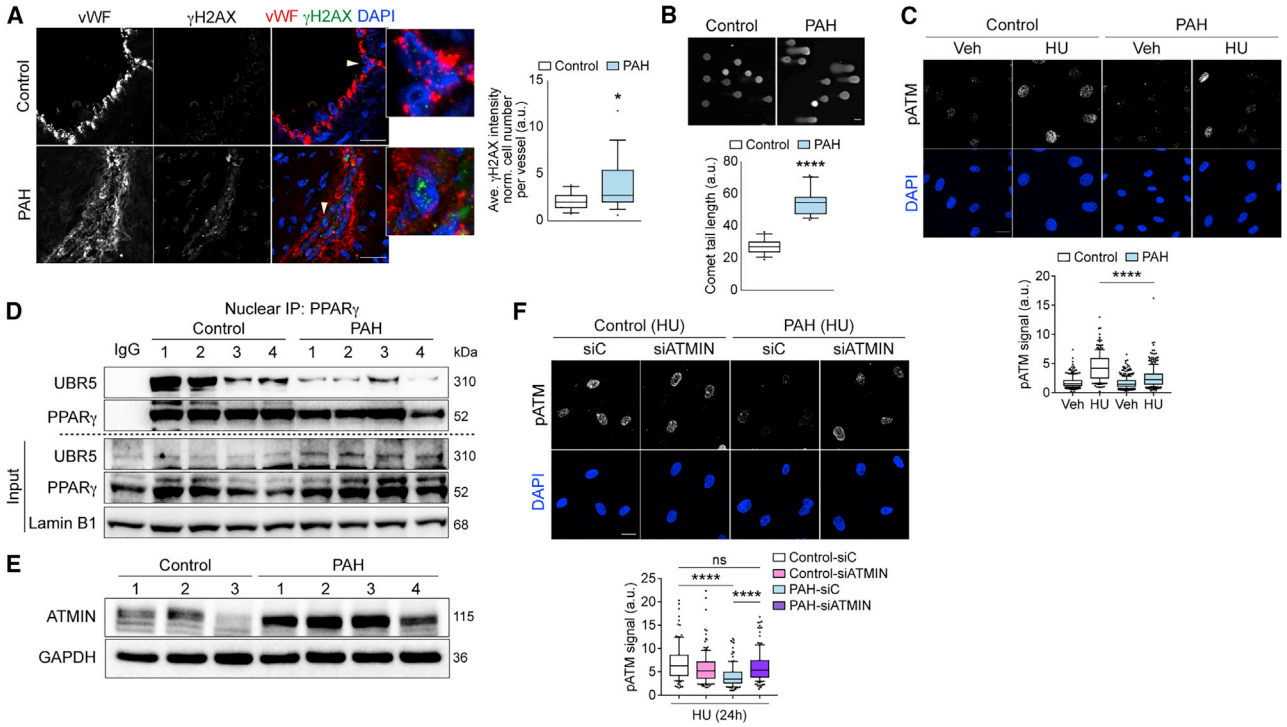

Figure 5. The PPARγ-ATMIN Axis Is Impaired in PAH-PAECs with Genomic Instability

(A) Confocal microscopy shows representative staining of γH2AX foci in PAECs (labeled by vWF) in lung tissue sections from pulmonary arterial hypertension (PAH) patients (18 vessels, 5 subjects) and controls (19 vessels, 6 subjects). Arrowheads indicate cells in insets.

(B) Representative comet assay of comet tail lengths in control and PAH-PAECs (n = 16 and 22, respectively).

(C) Confocal microscopy shows pATM foci in controls and PAH-PAECs with HU treatment (24 h).

(D) Representative immunoblots show nuclear endogenous interactions of PPARγ and UBR5 in controls and PAH-PAECs.

(E) Representative immunoblots show elevated ATMIN levels in PAH-PAECs compared to controls.

(F) Confocal microscopy shows pATM foci in controls and PAH-PAECs with siATMIN after HU treatment (24 h).

siC, siControl. The line in the box of the box and whisker plots marks the median and whiskers correspond to the 10th to 90th percentiles (A–C and F). Two-tailed Mann-Whitney test (A and B). Kruskal–Wallis ANOVA test with Dunn's test (C and F). *$p < 0.05$; ****$p < 0.0001$, ns., not significant. Scale bars, 5 μm (A); 20 μm (B, C, and E). See also Figure S6.

2010) or β-catenin (Alastalo et al., 2011). Since these interactions were established in adipocytes and ECs, they might be cell-type specific and undetectable in 293T cells. We uncovered previously unknown interactions with MRN and UBR5 that are relevant to 293T and ECs and, hence, are likely of biological significance in other PPARγ-expressing cell types. Supporting this contention is evidence that PPARγ synthetic ligands synergize with platinum-based drugs by activating the DDR pathway and inducing apoptosis of non-small-cell lung cancer cells (Girnun et al., 2007; Khandekar et al., 2018).

PPARγ DDR functions implicated by its binding partners MRN and UBR5 support the notion that novel cellular functions can be uncovered by understanding protein-protein interactions. Understanding the NBS1-PPARγ binding interface by using XL-MS and biochemical studies indicates that PPARγ DDR functions would require its DBD and LBD, similar to its non-canonical function in degrading nuclear factor κB (NF-κB)/p65 (Hou et al., 2012). We detected recently described PPARγ interactors, TR150 (Choi et al., 2014a; Khandekar et al., 2018). TR150 is part of the mediator complex, potentially involved in chromatin remodeling (Fondell et al., 1996). It also promotes PPARγ-mediated gene transcription (Choi et al., 2014a), as well as functions in RNA processing (Beli et al., 2012). Further study is warranted to investigate whether PPARγ is related to any of these functions.

DDR activation requires layers of control, including the ubiquitination pathway, to ensure rapid modifications and trans-localization of proteins (Mirzoeva and Petrini, 2001, 2003; Polo and Jackson, 2011). UBR5 belongs to the HECT (homology to E6-AP carboxyl terminus) family of E3 ubiquitin ligases that maintains its substrates at optimal levels for effective signaling transduction. Some of the UBR5 substrates include an ubiquitin ligase, RNF168 (Gudjonsson et al., 2012), a pro-apoptotic protein, MOAP-1 (Matsuura et al., 2017), and an ATM modulator, ATMIN (Zhang et al., 2014), which act independently in the DDR pathway. Here, we demonstrated that PPARγ is necessary for UBR5 ubiquitin ligase activity and potentially has a broad effect on other UBR5 substrates.

We focused on ATMIN because of its relationship with ATM, the nature of which has been context dependent (Liu et al., 2017; Schmidt et al., 2014; Zhang et al., 2014). We used prolonged HU treatment to induce replication stress-dependent double-strand breaks and, hence, ATM signaling. HU-induced

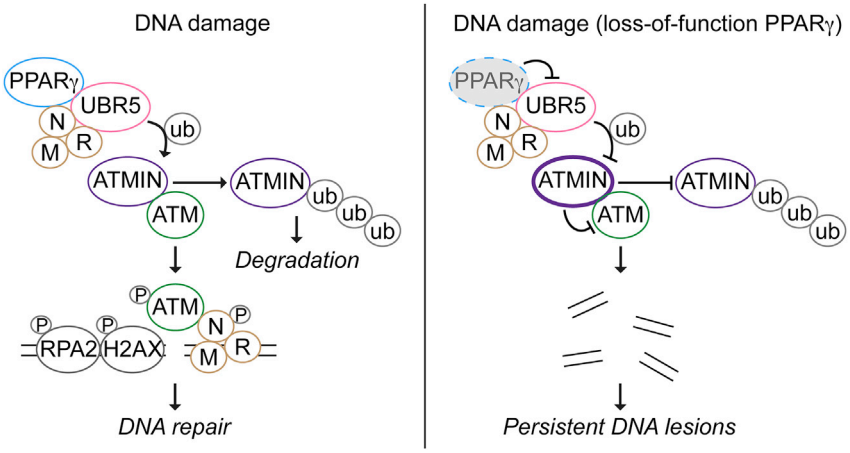

Figure 6. Proposed Model for PPARγ-Mediated DNA Damage Response Signaling

In response to DNA damage, ubiquitination of ATMIN is increased, leading to its proteasomal degradation to release ATM. ATM binds to NBS1 and is autophosphorylated (pATM) and recruited to the DNA lesions where ATM phosphorylates its targets, such as H2AX (γH2AX) and RPA2 (pRPA2) to facilitate DNA repair. Where there is a loss of function of PPARγ, ATMIN ubiquitination by UBR5 is inhibited; hence, ATMIN accumulates. This suppresses ATM activation and its signaling, eventually leading to persistent DNA lesions and genomic instability. P, phosphorylation; ub, ubiquitination.

damage also closely resembles chronic replication-induced genotoxic insults associated with genomic instability in vascular ECs from PAH patients (Aldred et al., 2010; de Jesus Perez et al., 2014). In both 293T and ECs, increased ATMIN resulting from silencing PPARγ or UBR5 inhibited ATM signaling. Importantly, depleting ATMIN in this context restored pATM and DNA repair. We demonstrated that PPARγ or UBR5-mediated ATMIN ubiquitination is associated with its proteasomal degradation. Others have shown that ionizing radiation-induced ATMIN ubiquitination (via UBR5) does not lead to degradation (Zhang et al., 2014). We propose that in response to the nature and duration of the DNA damage stimulus, the type and amount of ATMIN ubiquitination might vary, producing either degradative or a non-degradative response. This "ubiquitin threshold" model has been previously proposed (Swatek and Komander, 2016) and could account for our observations linking PPARγ and UBR5 to ATMIN ubiquitination and degradation. In addition, the C-terminal ATMIN SQ or TQ motif cluster domain could be highly modified, especially in response to DNA damage (Jurado et al., 2010). We postulate that the aberrant increase in ATMIN protein and possibly its modifications in PPARγ- and UBR5-depleted cells sterically inhibit ATM activation in response to DNA damage (Figure 6). Determining precisely how this occurs could lead to opportunities to selectively modulate the DDR pathway.

ATMIN was first identified as a transcription factor for *DYNLL1*. Both ATMIN and DYNLL1 are required for the initiation of lung budding during lung organogenesis (Goggolidou et al., 2014; Jurado et al., 2010). Distinguishing between ATMIN developmental and DDR functions by defining its targets of transcription or interacting partners would provide a greater understanding of ATMIN biology. Upstream of ATMIN, both PPARγ, and UBR5 knockout mice die in early embryonic life with developmental defects in the vasculature (Barak et al., 1999; Saunders et al., 2004). In the context of PAH, we postulate that the disrupted interactions between PPARγ and UBR5 would modulate the expression and activities of other substrates, which could be critical for EC function.

Our previous observations related to the role of PPARγ in the maintenance of endothelial homeostasis (Alastalo et al., 2011) and now in the DDR, coupled with an increasing body of evidence showing genomic instability and DNA damage in PAECs and smooth muscle cells from patients with PAH (Aldred et al., 2010; Meloche et al., 2014), led us to investigate whether PPARγ-mediated DNA damage sensing was impaired. PAH is a progressive disease associated with severe vascular occlusion owing to EC dysfunction, judged by propensity to apoptosis, inability to form tubes in culture (Sa et al., 2016), and cellular transformation (Hopper et al., 2016; Ranchoux et al., 2015). Our study indicates that the PPARγ-ATMIN axis is indeed perturbed in PAECs from PAH patients, with high ATMIN levels related to impaired DNA damage sensing and repair.

The common response of 293T cells and primary ECs further strengthens the notion that, perturbations in the PPARγ-UBR5-ATMIN axis could potentially occur in multiple cell types where PPARγ is expressed and, hence, would be applicable to a wide range of disease mechanisms.

STAR★METHODS

Detailed methods are provided in the online version of this paper and include the following:

- KEY RESOURCES TABLE
- CONTACT FOR REAGENT AND RESOURCE SHARING
- EXPERIMENTAL MODEL AND SUBJECT DETAILS
  - Cell culture
- METHOD DETAILS
  - siRNAs
  - Plasmids
  - Transient transfections
  - Nuclear extraction
  - Whole cell extraction
  - Immunoprecipitation
  - Denaturing immunoprecipitation
  - Immunoblotting
  - Size-exclusion chromatography
  - RNA extraction and quantitative PCR
  - Immunoprecipitation for mass spectrometry analyses
  - Mass spectrometry
  - Statistical analysis for AP-MS and TAP-MS

SUPPLEMENTAL INFORMATION

Supplemental Information includes six figures and six tables and can be found with this article online at https://doi.org/10.1016/j.celrep.2019.01.013.

ACKNOWLEDGMENTS

We thank A. Giaccia for helpful comments on the manuscript. We thank P. Griffin and T. Kamenecka (Scripps Research Institute, Florida) for providing PPARγ modulators; L. Nagy (University of Debrecen, Hungary), C. Craik (UCSF), N. Krogan (UCSF), H.-K. Lin (MD Anderson Cancer Center), and A. Behrens (King's College London) for providing plasmids; T. Desai (Stanford) for the use of the Leica confocal microscope; P.A. del Rosario (Stanford) for providing clinical information of the PHBI samples; and M. Fox and M. Roof (Stanford) for administrative assistance. We thank members of the Rabinovitch Lab and the Department of Radiation Oncology (Stanford) for their support. Mass spectrometry was performed at the Vincent Coates Foundation Mass Spectrometry Laboratory, Stanford University. Mass spectrometry was funded by award number S10RR027425 from the National Center For Research Resources. The Pulmonary Hypertension Breakthrough Initiative (PHBI) Network is funded by NIH/National Heath, Lung, and Blood Institute (NHLBI) R24 HL123767 and the Cardiovascular Medical Research and Education Fund (CMREF) grant UL1RR024986. This work was supported by NIH/NHLBI grant R01 HL087118 (M.R.), fellowships from the Deutsche Forschungsgemeinschaft (He 6855/1-1 to J.K.H. and Ni 1456/1-1 to N.P.N.), and from the Deutsche Herzstiftung e.V. (S/06/11 to I.D.).

AUTHOR CONTRIBUTIONS

C.G.L., C.M., and M.R. conceived the experiments; C.G.L. and M.R. interpreted all data and wrote the manuscript; C.G.L. performed most experiments; C.M. helped with cloning, immunoprecipitation, and data interpretation; N.M.S. performed immunofluorescence staining on tissue sections; E.V. carried out MS statistical analyses; V.K. performed the comet assay; D.L., O.A.-H., and M.E. performed PCR; J.K.H. helped with PCR; D.P.M. helped design experiments and provided PPARγ modulators; S.S. helped with primary cell cultures; F.G. performed size exclusion chromatography; L.W. and A.C. helped with isolation of PHBI lung cells; C.G. obtained animal tissue sections; J.S. and K.C. provided expertise on the DDR pathway; I.D., N.P.N., and M.K. provided help with animal experiments not included in the final version of manuscript; and all authors contributed to writing and provided feedback.

DECLARATION OF INTERESTS

The authors declare no competing interests.

Received: May 14, 2018
Revised: November 30, 2018
Accepted: January 3, 2019
Published January 29, 2019

REFERENCES

Ahmadian, M., Suh, J.M., Hah, N., Liddle, C., Atkins, A.R., Downes, M., and Evans, R.M. (2013). PPARγ signaling and metabolism: the good, the bad and the future. Nat. Med. *19*, 557–566.

Alastalo, T.P., Li, M., Perez, Vde.J., Pham, D., Sawada, H., Wang, J.K., Koskenvuo, M., Wang, L., Freeman, B.A., Chang, H.Y., and Rabinovitch, M. (2011). Disruption of PPARγ/β-catenin-mediated regulation of apelin impairs BMP-induced mouse and human pulmonary arterial EC survival. J. Clin. Invest. *121*, 3735–3746.

Aldred, M.A., Comhair, S.A., Varella-Garcia, M., Asosingh, K., Xu, W., Noon, G.P., Thistlethwaite, P.A., Tuder, R.M., Erzurum, S.C., Geraci, M.W., and Coldren, C.D. (2010). Somatic chromosome abnormalities in the lungs of patients with pulmonary arterial hypertension. Am. J. Respir. Crit. Care Med. *182*, 1153–1160.

Barak, Y., Nelson, M.C., Ong, E.S., Jones, Y.Z., Ruiz-Lozano, P., Chien, K.R., Koder, A., and Evans, R.M. (1999). PPAR gamma is required for placental, cardiac, and adipose tissue development. Mol. Cell *4*, 585–595.

Beli, P., Lukashchuk, N., Wagner, S.A., Weinert, B.T., Olsen, J.V., Baskcomb, L., Mann, M., Jackson, S.P., and Choudhary, C. (2012). Proteomic investigations reveal a role for RNA processing factor THRAP3 in the DNA damage response. Mol. Cell *46*, 212–225.

Burma, S., Chen, B.P., Murphy, M., Kurimasa, A., and Chen, D.J. (2001). ATM phosphorylates histone H2AX in response to DNA double-strand breaks. J. Biol. Chem. *276*, 42462–42467.

Chandra, V., Huang, P., Hamuro, Y., Raghuram, S., Wang, Y., Burris, T.P., and Rastinejad, F. (2008). Structure of the intact PPAR-gamma-RXR- nuclear receptor complex on DNA. Nature *456*, 350–356.

Cheng, K.C., Cahill, D.S., Kasai, H., Nishimura, S., and Loeb, L.A. (1992). 8-Hydroxyguanine, an abundant form of oxidative DNA damage, causes G—T and A—C substitutions. J. Biol. Chem. *267*, 166–172.

Choi, J.H., Choi, S.S., Kim, E.S., Jedrychowski, M.P., Yang, Y.R., Jang, H.J., Suh, P.G., Banks, A.S., Gygi, S.P., and Spiegelman, B.M. (2014a). Thrap3 docks on phosphoserine 273 of PPARγ and controls diabetic gene programming. Genes Dev. *28*, 2361–2369.

Choi, M., Chang, C.Y., Clough, T., Broudy, D., Killeen, T., MacLean, B., and Vitek, O. (2014b). MSstats: an R package for statistical analysis of quantitative mass spectrometry-based proteomic experiments. Bioinformatics *30*, 2524–2526.

Cox, J., and Mann, M. (2008). MaxQuant enables high peptide identification rates, individualized p.p.b.-range mass accuracies and proteome-wide protein quantification. Nat. Biotechnol. *26*, 1367–1372.

Cuadrado, M., Martinez-Pastor, B., Murga, M., Toledo, L.I., Gutierrez-Martinez, P., Lopez, E., and Fernandez-Capetillo, O. (2006). ATM regulates ATR chromatin loading in response to DNA double-strand breaks. J. Exp. Med. *203*, 297–303.

de Jesus Perez, V.A., Yuan, K., Lyuksyutova, M.A., Dewey, F., Orcholski, M.E., Shuffle, E.M., Mathur, M., Yancy, L., Jr., Rojas, V., Li, C.G., et al. (2014). Whole-exome sequencing reveals TopBP1 as a novel gene in idiopathic pulmonary arterial hypertension. Am. J. Respir. Crit. Care Med. *189*, 1260–1272.

Diebold, I., Hennigs, J.K., Miyagawa, K., Li, C.G., Nickel, N.P., Kaschwich, M., Cao, A., Wang, L., Reddy, S., Chen, P.I., et al. (2015). BMPR2 preserves mitochondrial function and DNA during reoxygenation to promote endothelial cell survival and reverse pulmonary hypertension. Cell Metab. *21*, 596–608.

Duval, C., Chinetti, G., Trottein, F., Fruchart, J.C., and Staels, B. (2002). The role of PPARs in atherosclerosis. Trends Mol. Med. *8*, 422–430.

Fondell, J.D., Ge, H., and Roeder, R.G. (1996). Ligand induction of a transcriptionally active thyroid hormone receptor coactivator complex. Proc. Natl. Acad. Sci. USA *93*, 8329–8333.

Girnun, G.D., Naseri, E., Vafai, S.B., Qu, L., Szwaya, J.D., Bronson, R., Alberta, J.A., and Spiegelman, B.M. (2007). Synergy between PPARgamma ligands and platinum-based drugs in cancer. Cancer Cell *11*, 395–406.

Glickman, M.H., and Ciechanover, A. (2002). The ubiquitin-proteasome proteolytic pathway: destruction for the sake of construction. Physiol. Rev. *82*, 373–428.

Goggolidou, P., Stevens, J.L., Agueci, F., Keynton, J., Wheway, G., Grimes, D.T., Patel, S.H., Hilton, H., Morthorst, S.K., DiPaolo, A., et al. (2014). ATMIN is a transcriptional regulator of both lung morphogenesis and ciliogenesis. Development *141*, 3966–3977.

Gudjonsson, T., Altmeyer, M., Savic, V., Toledo, L., Dinant, C., Grøfte, M., Bartkova, J., Poulsen, M., Oka, Y., Bekker-Jensen, S., et al. (2012). TRIP12 and UBR5 suppress spreading of chromatin ubiquitylation at damaged chromosomes. Cell *150*, 697–709.

Guignabert, C., Alvira, C.M., Alastalo, T.P., Sawada, H., Hansmann, G., Zhao, M., Wang, L., El-Bizri, N., and Rabinovitch, M. (2009). Tie2-mediated loss of peroxisome proliferator-activated receptor-gamma in mice causes PDGF receptor-beta-dependent pulmonary arterial muscularization. Am. J. Physiol. Lung Cell. Mol. Physiol. *297*, L1082–L1090.

Hamblin, M., Chang, L., Zhang, H., Yang, K., Zhang, J., and Chen, Y.E. (2010). Vascular smooth muscle cell peroxisome proliferator-activated receptor-γ deletion promotes abdominal aortic aneurysms. J. Vasc. Surg. *52*, 984–993.

Hammond, E.M., Dorie, M.J., and Giaccia, A.J. (2003). ATR/ATM targets are phosphorylated by ATR in response to hypoxia and ATM in response to reoxygenation. J. Biol. Chem. *278*, 12207–12213.

Hansmann, G., de Jesus Perez, V.A., Alastalo, T.P., Alvira, C.M., Guignabert, C., Bekker, J.M., Schellong, S., Urashima, T., Wang, L., Morrell, N.W., and Rabinovitch, M. (2008). An antiproliferative BMP-2/PPARgamma/apoE axis in human and murine SMCs and its role in pulmonary hypertension. J. Clin. Invest. *118*, 1846–1857.

Hopper, R.K., Moonen, J.R., Diebold, I., Cao, A., Rhodes, C.J., Tojais, N.F., Hennigs, J.K., Gu, M., Wang, L., and Rabinovitch, M. (2016). In pulmonary arterial hypertension, reduced BMPR2 promotes endothelial-to-mesenchymal transition via HMGA1 and its target slug. Circulation *133*, 1783–1794.

Hou, Y., Moreau, F., and Chadee, K. (2012). PPARγ is an E3 ligase that induces the degradation of NFκB/p65. Nat. Commun. *3*, 1300.

Jurado, S., Smyth, I., van Denderen, B., Tenis, N., Hammet, A., Hewitt, K., Ng, J.L., McNees, C.J., Kozlov, S.V., Oka, H., et al. (2010). Dual functions of ASCIZ in the DNA base damage response and pulmonary organogenesis. PLoS Genet. *6*, e1001170.

Khandekar, M.J., Banks, A.S., Laznik-Bogoslavski, D., White, J.P., Choi, J.H., Kazak, L., Lo, J.C., Cohen, P., Wong, K.K., Kamenecka, T.M., et al. (2018). Noncanonical agonist PPARγ ligands modulate the response to DNA damage and sensitize cancer cells to cytotoxic chemotherapy. Proc. Natl. Acad. Sci. USA *115*, 561–566.

Koppen, A., and Kalkhoven, E. (2010). Brown vs white adipocytes: the PPARgamma coregulator story. FEBS Lett. *584*, 3250–3259.

Kurz, E.U., Douglas, P., and Lees-Miller, S.P. (2004). Doxorubicin activates ATM-dependent phosphorylation of multiple downstream targets in part through the generation of reactive oxygen species. J. Biol. Chem. *279*, 53272–53281.

Lee, J.H., and Paull, T.T. (2004). Direct activation of the ATM protein kinase by the Mre11/Rad50/Nbs1 complex. Science *304*, 93–96.

Leszczynska, K.B., Göttgens, E.L., Biasoli, D., Olcina, M.M., Lent, J., Anbalagan, S., Bernhardt, S., Giaccia, A.J., and Hammond, E.M. (2016). Mechanisms and consequences of ATMIN repression in hypoxic conditions: roles for p53 and HIF-1. Sci. Rep. *6*, 21698.

Liu, S., Opiyo, S.O., Manthey, K., Glanzer, J.G., Ashley, A.K., Amerin, C., Troksa, K., Shrivastav, M., Nickoloff, J.A., and Oakley, G.G. (2012). Distinct roles for DNA-PK, ATM and ATR in RPA phosphorylation and checkpoint activation in response to replication stress. Nucleic Acids Res. *40*, 10780–10794.

Liu, R., King, A., Hoch, N.C., Chang, C., Kelly, G.L., Deans, A.J., and Heierhorst, J. (2017). ASCIZ/ATMIN is dispensable for ATM signaling in response to replication stress. DNA Repair (Amst.) *57*, 29–34.

Marciano, D.P., Kuruvilla, D.S., Boregowda, S.V., Asteian, A., Hughes, T.S., Garcia-Ordonez, R., Corzo, C.A., Khan, T.M., Novick, S.J., Park, H., et al. (2015). Pharmacological repression of PPARγ promotes osteogenesis. Nat. Commun. *6*, 7443.

Matsuura, K., Huang, N.J., Cocce, K., Zhang, L., and Kornbluth, S. (2017). Downregulation of the proapoptotic protein MOAP-1 by the UBR5 ubiquitin ligase and its role in ovarian cancer resistance to cisplatin. Oncogene *36*, 1698–1706.

Meloche, J., Pflieger, A., Vaillancourt, M., Paulin, R., Potus, F., Zervopoulos, S., Graydon, C., Courboulin, A., Breuils-Bonnet, S., Tremblay, E., et al. (2014). Role for DNA damage signaling in pulmonary arterial hypertension. Circulation *129*, 786–797.

Mirzoeva, O.K., and Petrini, J.H. (2001). DNA damage-dependent nuclear dynamics of the Mre11 complex. Mol. Cell. Biol. *21*, 281–288.

Mirzoeva, O.K., and Petrini, J.H. (2003). DNA replication-dependent nuclear dynamics of the Mre11 complex. Mol. Cancer Res. *1*, 207–218.

Polo, S.E., and Jackson, S.P. (2011). Dynamics of DNA damage response proteins at DNA breaks: a focus on protein modifications. Genes Dev. *25*, 409–433.

Rabinovitch, M. (2010). PPARgamma and the pathobiology of pulmonary arterial hypertension. Adv. Exp. Med. Biol. *661*, 447–458.

Rabinovitch, M. (2012). Molecular pathogenesis of pulmonary arterial hypertension. J. Clin. Invest. *122*, 4306–4313.

Ranchoux, B., Antigny, F., Rucker-Martin, C., Hautefort, A., Péchoux, C., Bogaard, H.J., Dorfmüller, P., Remy, S., Lecerf, F., Planté, S., et al. (2015). Endothelial-to-mesenchymal transition in pulmonary hypertension. Circulation *131*, 1006–1018.

Reinhardt, H.C., and Yaffe, M.B. (2013). Phospho-Ser/Thr-binding domains: navigating the cell cycle and DNA damage response. Nat. Rev. Mol. Cell Biol. *14*, 563–580.

Sa, S., Gu, M., Chappell, J., Shao, N.Y., Ameen, M., Elliott, K.A., Li, D., Grubert, F., Li, C.G., Taylor, S., et al. (2016). iPSC model of pulmonary arterial hypertension reveals novel gene expression and patient specificity. Am. J. Respir. Crit. Care Med. *195*, 930–941.

Saunders, D.N., Hird, S.L., Withington, S.L., Dunwoodie, S.L., Henderson, M.J., Biben, C., Sutherland, R.L., Ormandy, C.J., and Watts, C.K. (2004). Edd, the murine hyperplastic disc gene, is essential for yolk sac vascularization and chorioallantoic fusion. Mol. Cell. Biol. *24*, 7225–7234.

Schmidt, L., Wiedner, M., Velimezi, G., Prochazkova, J., Owusu, M., Bauer, S., and Loizou, J.I. (2014). ATMIN is required for the ATM-mediated signaling and recruitment of 53BP1 to DNA damage sites upon replication stress. DNA Repair (Amst.) *24*, 122–130.

Schneider, C.A., Rasband, W.S., and Eliceiri, K.W. (2012). NIH Image to ImageJ: 25 years of image analysis. Nat. Methods *9*, 671–675.

Smoot, M.E., Ono, K., Ruscheinski, J., Wang, P.L., and Ideker, T. (2011). Cytoscape 2.8: new features for data integration and network visualization. Bioinformatics *27*, 431–432.

Swatek, K.N., and Komander, D. (2016). Ubiquitin modifications. Cell Res. *26*, 399–422.

Vattulainen-Collanus, S., Akinrinade, O., Li, M., Koskenvuo, M., Li, C.G., Rao, S.P., de Jesus Perez, V., Yuan, K., Sawada, H., Koskenvuo, J.W., et al. (2016). Loss of PPARγ in endothelial cells leads to impaired angiogenesis. J. Cell Sci. *129*, 693–705.

Vinayagam, A., Hu, Y., Kulkarni, M., Roesel, C., Sopko, R., Mohr, S.E., and Perrimon, N. (2013). Protein complex-based analysis framework for high-throughput data sets. Sci. Signal. *6*, rs5.

Wiśniewski, J.R., Zougman, A., Nagaraj, N., and Mann, M. (2009). Universal sample preparation method for proteome analysis. Nat. Methods *6*, 359–362.

Wu, J., Zhang, X., Zhang, L., Wu, C.Y., Rezaeian, A.H., Chan, C.H., Li, J.M., Wang, J., Gao, Y., Han, F., et al. (2012). Skp2 E3 ligase integrates ATM activation and homologous recombination repair by ubiquitinating NBS1. Mol. Cell *46*, 351–361.

Yazdi, P.T., Wang, Y., Zhao, S., Patel, N., Lee, E.Y., and Qin, J. (2002). SMC1 is a downstream effector in the ATM/NBS1 branch of the human S-phase checkpoint. Genes Dev. *16*, 571–582.

Zhang, T., Penicud, K., Bruhn, C., Loizou, J.I., Kanu, N., Wang, Z.Q., and Behrens, A. (2012). Competition between NBS1 and ATMIN controls ATM signaling pathway choice. Cell Rep. *2*, 1498–1504.

Zhang, T., Cronshaw, J., Kanu, N., Snijders, A.P., and Behrens, A. (2014). UBR5-mediated ubiquitination of ATMIN is required for ionizing radiation-induced ATM signaling and function. Proc. Natl. Acad. Sci. USA *111*, 12091–12096.

Ziv, Y., Bielopolski, D., Galanty, Y., Lukas, C., Taya, Y., Schultz, D.C., Lukas, J., Bekker-Jensen, S., Bartek, J., and Shiloh, Y. (2006). Chromatin relaxation in response to DNA double-strand breaks is modulated by a novel ATM- and KAP-1 dependent pathway. Nat. Cell Biol. *8*, 870–876.

STAR★METHODS

KEY RESOURCES TABLE

REAGENT or RESOURCE	SOURCE	IDENTIFIER
Antibodies		
Monoclonal ANTI-FLAG® M2 antibody	Sigma-Aldrich	Cat#F1804, RRID:AB_262044
Anti-Strep Tag antibody [GT661]	Abcam	Cat#ab184224
Mre11 Antibody	Novus	Cat#NB100-142, RRID:AB_10077796
Rad50 (13B3/2C6) antibody	Santa Cruz Biotechnology	Cat#sc-56209, RRID:AB_785402
NBS1 Antibody	Novus	Cat#NB100-221, RRID:AB_10001212
RXRalpha (D-20) antibody	Santa Cruz Biotechnology	Cat#sc-553, RRID:AB_2184874
UBR5/EDD1 Antibody	Bethyl	Cat#A300-573A, RRID:AB_2210189
Anti-ATM Protein Kinase pS1981 (MOUSE) Monoclonal Antibody	Rockland	Cat#200-301-400, RRID:AB_217868
ATM antibody	Abcam	Cat#ab2631, RRID:AB_2062948
PPAR (D69) Antibody	Cell Signaling Technology	Cat#2430, RRID:AB_823599
Anti-ASCIZ/ATMIN antibody	Millipore	Cat#AB3271, RRID:AB_2243333
Phospho RPA32 (S4/S8) Antibody	Bethyl	Cat#A300-245A, RRID:AB_210547
RPA32 Antibody	Bethyl	Cat#A300-244A, RRID:AB_185548
Phospho KAP-1 (S824) Antibody	Bethyl	Cat# A300-767A, RRID:AB_669740
KAP-1 Antibody	Bethyl	Cat#A303-838A, RRID:AB_2620189
Phospho SMC1 (S966) Antibody	Bethyl	Cat#A300-050A, RRID:AB_67578
SMC1 Antibody	Bethyl	Cat#A303-834A, RRID:AB_2620185
Mouse Anti-HA.11 Monoclonal Antibody, Unconjugated, Clone 16B12	Covance Research Products Inc	Cat#MMS-101P-500, RRID:AB_291261
Mouse Anti-Histone H2A.X, phospho (Ser139) Monoclonal antibody, Unconjugated, Clone jbw301	Millipore	Cat#05-636, RRID:AB_309864
H2AX Antibody	Bethyl	Cat#A300-083A, RRID:AB_203289
Von Willebrand Factor antibody	Abcam	Cat#ab6994, RRID:AB_305689
PPARG / PPAR Gamma Antibody (phospho-Ser245/273)	LS Bio	Cat#LS-C209422
K48-linkage Specific Polyubiquitin Antibody	Cell Signaling Technology	Cat#4289, RRID:AB_10557239
Mouse Anti-8-oxo-dG Monoclonal Antibody, Unconjugated, Clone 200	R and D Systems	Cat#4354-MC-050, RRID:AB_1857195
Lamin B1 (S-20) antibody	Santa Cruz Biotechnology	Cat#sc-30264, RRID:AB_2136305
Mouse Anti-Glyceraldehyde-3-PDH (GAPDH) Monoclonal antibody, Unconjugated	Millipore	Cat#MAB374, RRID:AB_2107445
Rat Anti-ORC2 Monoclonal Antibody, Unconjugated, Clone 3G6	Cell Signaling Technology	Cat#4736, RRID:AB_2157716
Mouse Anti-alpha-Tubulin Monoclonal Antibody, Unconjugated, Clone B-5-1-2	Sigma-Aldrich	Cat#T6074, RRID:AB_477582
Rabbit anti-Goat IgG (H+L) Secondary Antibody, HRP	Thermo Fisher Scientific	Cat#81-1620, RRID:AB_2534006)
Goat anti-Rat IgG (H+L) Secondary Antibody, HRP	Thermo Fisher Scientific	Cat#31470, RRID:AB_228356
Peroxidase-IgG Fraction Monoclonal Mouse Anti-Rabbit IgG, Light Chain Specific (min X Bov,Gt,Arm Hms,Hrs,Hu,Ms,Rat,Shp Ig) antibody	Jackson ImmunoResearch Labs	Cat#211-032-171, RRID:AB_2339149
Peroxidase-AffiniPure Goat Anti-Mouse IgG, Light Chain* Specific (min X Bov,Gt,Hrs,Hu,Rb,Rat,Shp Ig) antibody	Jackson ImmunoResearch Labs	Cat#115-035-174, RRID:AB_2338512

(*Continued on next page*)

Continued

REAGENT or RESOURCE	SOURCE	IDENTIFIER
Donkey anti-Mouse IgG (H+L) Highly Cross-Adsorbed Secondary Antibody, Alexa Fluor 488	Thermo Fisher Scientific	Cat#A-21202, RRID:AB_141607
Donkey anti-Rabbit IgG (H+L) Highly Cross-Adsorbed Secondary Antibody, Alexa Fluor 594	Thermo Fisher Scientific	Cat#A-21207, RRID:AB_141637
Biological Samples		
Human control and PAH patient specimens (tissues and cells)	The Pulmonary Hypertension Breakthrough Initiative (PHBI) Network	Table S5
Chemicals, Peptides, and Recombinant Proteins		
PolyJet *In Vitro* DNA Transfection Reagent	SignaGen Laboratories	Cat#SL100688
Lipofectamine RNAiMAX Transfection Reagent	Thermo Fisher Scientific	Cat#13778150
GW9662	Sigma-Aldrich	Cat#M6191
SR10221	Drs. Patrick Griffin, Theodore Kamenecka, Scripps Research Institute, Florida	Marciano et al., 2015
	Sigma-Aldrich	Cat#D1515
HU	Sigma-Aldrich	Cat#H8627
BS3 (bis(sulfosuccinimidyl)suberate)	Thermo Fisher Scientific	Cat#21580
ChromPure Rabbit IgG, whole molecule	Jackson ImmunoResearch Labs	Cat#011-000-003
ChromPure Rabbit IgG, whole molecule	Jackson ImmunoResearch Labs	Cat#015-000-003
MG-132	Calbiochem	Cat#474790
NEM (N-ethylmaleimide)	Thermo Fisher Scientific	Cat#23030
Flag Peptide	Sigma-Aldrich	Cat#F3290
Critical Commercial Assays		
Click-iT EdU Alexa Fluor 647 Flow Cytometry Assay Kit	Thermo Fisher Scientific	***Cat#C10634***
CometAssay Reagent Kit for Single Cell Gel Electrophoresis Assay	Trevigen	Cat#4250-050-K
P5 Primary Cell 4D-Nucleofector X Kit L	Lonza	Cat#V4XP-5024
Deposited Data		
Raw mass spectrometry data	https://massive.ucsd.edu/ProteoSAFe/dataset.jsp?task=d597007ca8d7436587ccc4a7d4848842	Accession number: MSV000083257
PPARγ and RXRα structure	Chandra et al., 2008	PDB ID: 3DZU
Experimental Models: Cell Lines		
Human: 293T	ATCC	Cat#CRL-3216
Human PAECs	PromoCell	Cat#C-12241
Human umbilical vein ECs	Angio-Proteomie	Cat#cAP-0001GFP
Experimental Models: Organisms/Strains		
Mouse: *Tie2-PPARγ*$^{-/-}$ tissue specimens	Guignabert et al., 2009	Guignabert et al., 2009
Oligonucleotides		
siRNA targeting sequence (pool): PPARγ	Dharmacon	Cat#L-003436-00-0005
siRNA targeting sequence (#9): PPARγ	Dharmacon	Cat#J-003436-09-0005
siRNA targeting sequence (pool): UBR5	Dharmacon	Cat#M-007189-02-0010
siRNA targeting sequence (pool): ATMIN	Dharmacon	Cat#L-020304-01-0010
siRNA targeting sequence (pool): NBS1	Dharmacon	Cat#M-009641-02-0005
siRNA targeting sequence (pool): Non-targeting	Dharmacon	Cat#D-001810-10
Primers for quantitative real-time PCR and cloning	This paper	Table S6
Recombinant DNA		
Plasmid: pCMV2-Flag-PPARγ1	This paper	N/A
Plasmid: pCMV2-Flag-PPARγ1-LBD	This paper	N/A

(*Continued on next page*)

Continued

REAGENT or RESOURCE	SOURCE	IDENTIFIER
Plasmid: pcDNA-PPARγ1-2xStrep	This paper	N/A
Plasmid: pcDNA3-NBS1	Dr. Hui-Kuan Lin, University of Texas MD Anderson Cancer Center	Wu et al., 2012
Plasmid: pCMV2-siRNA-resistant-Flag-PPARγ1 (siRES-PPARγ)	This paper	N/A
Plasmid: pCMVtag2B-Flag-ATMIN (1-354)	Dr. Axel Behrens, King's College London	Zhang et al., 2014
Plasmid: pCMV2-siRNA-resistant-Flag-PPARγ1 (siRES-PPARγ)	This paper	N/A
Plasmid: pcDNA-GFP-StrepFlag	Dr. Nevan Krogan, UCSF	N/A
Plasmid: HA-ubiquitin	Dr. Nevan Krogan, UCSF	N/A
Software and Algorithms		
MaxQuant	Cox and Mann, 2008	http://www.coxdocs.org/doku.php?id=maxquant:common:download_and_installation#download
MSstats	Choi et al., 2014b	https://www.bioconductor.org/packages/release/bioc/html/MSstats.html
COMPLEAT	Vinayagam et al., 2013	http://www.flyrnai.org/compleat/
Ingenuity Pathway Analysis	QIAGEN	https://www.qiagenbioinformatics.com/products/ingenuity-pathway-analysis/
Cytoscape	Smoot et al., 2011	https://cytoscape.org/
Byonic	Protein Metrics	https://www.proteinmetrics.com/products/byonic/
Byologic	Protein Metrics	https://www.proteinmetrics.com/products/byologic/
PyMOL Molecular Graphical System	Schrödinger, LCC	https://pymol.org/2/
ImageJ	NIH	https://imagej.nih.gov/ij/
Comet Assay Plugin for ImageJ	Dr. Robert Bagnell, University of North Carolina	https://www.med.unc.edu/microscopy/resources/imagej-plugins-and-macros/comet-assay
GraphPad Prism	GraphPad Software	https://www.graphpad.com/scientific-software/prism/

CONTACT FOR REAGENT AND RESOURCE SHARING

Further information and requests for reagents should be directed to and will be fulfilled by the Lead Contact, Marlene Rabinovitch (marlener@stanford.edu).

EXPERIMENTAL MODEL AND SUBJECT DETAILS

Cell culture

293T cells (ATCC) were maintained in Dulbecco's Modified Eagle's Medium (DMEM, GIBCO) supplemented with 10% fetal bovine serum (FBS, GIBCO) and penicillin/streptomycin (GIBCO). Commercially available primary human PAECs (PromoCell) and umbilical vein ECs (HUVEC) (Angio-Proteomie) were cultured in complete EC medium (ScienCell). Primary human PAEC were purified from explanted lungs of patients undergoing transplantation due to PAH, or from controls (unused donors) obtained with approval from the Pulmonary Hypertension Breakthrough Initiative (PHBI) Network (see Acknowledgments). The PAEC were isolated by scraping the endothelial layer of pulmonary arteries and cultured in complete EC medium. Once PAEC cultures were established from explanted lungs, EC were further purified by incubating the cell suspension in complete EC medium with CD31 Dynabeads (Thermo Fisher Scientific) for 10 min at room temperature, followed by three washes in phosphate-buffered saline (PBS, GIBCO), resuspended and re-cultured in complete EC medium. Demographic information for patient and control (unused donor) lungs is provided in Table S5. In this study, PAEC isolated from small (< 1 mm) and large pulmonary arteries were used between passages 4-8 with similar distribution when comparing controls and PAH. All cultures were tested negative for mycoplasma contamination. Further details can be found in Supplemental Information.

METHOD DETAILS

siRNAs

ON-TARGETplus SMARTpool siRNA targeting PPARγ (L-003436-00-0005; Dharmacon) was used to deplete PPARγ for all experiments. For verifying γH2AX suppression, individual siRNA of the pool were used (#7, J-003436-07-0005; #8, J-003436-08-0005; #9, J-003436-09-0005, Dharmacon). For depleting UBR5, we used siGENOME SMARTpool siRNA targeting UBR5 (M-007189-02-0010, Dharmacon). For depleting ATMIN, we used ON-TARGETplus SMARTpool siRNA targeting ATMIN (L-020304-01-0010, Dharmacon). ON-TARGETplus non-targeting pool (D-001810-10-05, Dharmacon) was used for all siControl transfections.

Plasmids

An amino-terminal Flag tagged-PPARγ1 (courtesy of Dr. László Nagy, University of Debrecen, Hungary) was mutagenized to achieve 100% identity to the published sequence (NM_005037) using site-directed mutagenesis via a quick-change PCR (QC-PCR) protocol. Deletion of the PPARγ LBD was generated using the QC-PCR protocol. Flag-PPARγ plasmids were amplified using PfuUltra (Agilent) and primers that introduce a stop codon to delete PPARγ LBD (Table S6). Products were DpnI (NEB) digested then transformed into One Shot TOP10 cells (Thermo Fisher Scientific). For generating the carboxyl-terminal 2xStrep tagged-PPARγ, the PPARγ open reading frame was amplified with primers to create EcoRI and NotI flanking sites (Table S6). PCR product was inserted into the pcDNA 2xStrep vector following the In-Fusion HD Cloning Kit protocol (Clontech). For generating the Flag-PPARγ siRNA resistant construct, primers were used to generate three silent mutations in the PPARγ siRNA#9 targeted region: GACAGCGACTTGGCAATAT (Table S6). The silent mutations introduced are underlined: GACAGCGATCTCGCAATAT. The carboxyl-terminal StrepFlag-tagged GFP, 2xStrep pcDNA plasmids and the amino-terminal HA-tagged ubiquitin were kindly provided to us by Dr. Nevan Krogan, UCSF. The amino-terminal Flag tagged-NBS1 was kindly provided by Dr. Hui-Kuan Lin, University of Texas MD Anderson Cancer Center. The amino-terminal Flag tagged-ATMIN (amino acids 1-354) was kindly provided by Dr. Axel Behrens, King's College London. pCMV2-Flag (Sigma) was used as vector control.

Transient transfections

Plasmids were transfected into 293T cells using PolyJet at 3:1 (polyjet:DNA) according to the manufacturer's instructions (SignaGen Laboratories). siRNAs were transfected into 293T using Lipofectamine RNAiMAX (Invitrogen). In primary PAEC, siRNAs or plasmid DNA were transfected using P5 Primary Cell 4D-Nucleofector X Kit (Lonza) according to manufacturer's instructions (Lonza).

Nuclear extraction

Cells were washed and scraped in ice-cold Tris-buffered saline (TBS, Corning). Cell pellets were resuspended in hypotonic buffer [10 mM HEPES, pH 7.9, 10 mM KCl, 1.5 mM $MgCl_2$, Halt protease and phosphatase inhibitor (Thermo Scientific)], and homogenized 10 times using a dounce homogenizer (pestle B) (Kimble Chase). The nuclei were then pelleted by centrifugation at 13,000 rpm at 4°C for 5 min, and lysed in high salt buffer [20 mM HEPES, pH 7.9, 0.42 M NaCl, 25% glycerol, 5 mM $CaCl_2$, 1.5 mM $MgCl_2$, 0.1% Nonidet P-40 (NP-40), 0.2 mM EDTA, Halt protease and phosphatase inhibitor]. Lysates were homogenized 20 times using a dounce homogenizer (pestle B), and incubated with micrococcal nuclease (Thermo Scientific) at room temperature for 15 min to further digest chromatin. Nuclear extracts were collected by centrifugation at 14,000 rpm at 4°C for 20 min. For immunoprecipitation, lysates were diluted with 3x volumes of low detergent buffer (20 mM HEPES, pH 7.9, 1 mM EDTA, 0.2% NP-40, Halt protease and phosphatase inhibitor).

Whole cell extraction

For whole-cell extract for immunoprecipitation, cells were washed in ice-cold TBS, lysed in 0.2% NP-40 buffer (50 mM Tris-HCl, pH 8.0, 150 mM NaCl, 5 mM $CaCl_2$, 1 mM EDTA, 0.2% NP-40, Halt protease and phosphatase inhibitor), and incubated on ice for 15 min. Lysates were homogenized 20 times using a dounce homogenizer (pestle B), and incubated with micrococcal nuclease as described above. Cell extracts were collected by centrifugation at 14,000 rpm at 4°C for 20 min. For protein analyses, cells were washed in ice-cold TBS, and lysed in RIPA buffer (50 mM Tris-HCl, pH 8.0, 150 mM NaCl, 5 mM $CaCl_2$, 1% NP-40, 0.5% sodium deoxycholate, 0.1% SDS, Halt protease and phosphatase inhibitor). Cell extracts were incubated with micrococcal nuclease at room temperature for 15 min, and collected as described above.

Immunoprecipitation

Diluted nuclear extracts or undiluted whole cell extracts were incubated with antibodies overnight at 4°C with rotation. The next day, Protein-G Dynabeads (Thermo Fisher Scientific) were added to cell extracts containing antibodies, and incubated for 3 h at 4°C with rotation. After incubation, beads were washed three times in ice-cold wash buffer (50 mM Tris-HCl, pH 7.5, 150 mM NaCl, 1 mM EDTA, 0.05% NP-40). Proteins were eluted in acid using IgG elution buffer (Thermo Scientific) at room temperature for 10 min on gentle vortex. The final elution was collected and neutralized with 1/10 volume of 1 M Tris-HCl, pH 9.0.

Denaturing immunoprecipitation

293T cells were preincubated with MG132 (10 μM) for 2 hours. Cells were then washed in ice-cold TBS containing N-ethylmaleimide (10 mM, Thermo Fisher Scientific). Cells were immediately lysed in boiled 1% SDS buffer (50 mM Tris-HCl, pH 8.0 and 1% SDS), and incubated at 95°C for 20 min. Cell extracts were collected by centrifugation at 14,000 rpm for 20 min. Cell extracts were diluted with 3x volumes of dilution buffer (50 mM Tris-HCl, pH 8.0, 150 mM NaCl, Halt protease and phosphatase inhibitor), and proceeded with immunoprecipitation protocol described above. Proteins were eluted by incubating beads in 2x Laemmli sample buffer (Bio-Rad) containing TCEP, at 95°C for 10 min.

Immunoblotting

Equal amounts of proteins, measured by BCA assay (Thermo Scientific), were mixed with sample buffers (NuPAGE LDS Sample Buffer, Thermo Fisher Scientific; Laemmli Protein Sample Buffer, Bio-Rad) containing TCEP (Pierce) and were separated by SDS-PAGE on 4%–12% Bis-Tris gels (Thermo Fisher Scientific) for 15-70 kDa proteins or 4%–20% Tris-Glycine gels (Bio-Rad) for 30-350 kDa proteins and transferred onto PVDF membranes (Bio-Rad) using the wet transfer system (Bio-Rad). Bis-Tris gels were transferred in NuPAGE transfer buffer (Novex) containing 20% methanol. Tris-Glycine gels were transferred in Tris-Glycine buffer containing 5% methanol and 0.01% SDS. Membranes were blocked with 5% bovine serum albumin (BSA; Research Products International) in TBST (0.1% (v/v) Tween-20) at room temperature for 1 h. Primary antibody incubations were carried out in the blocking buffer at 4°C overnight, and secondary antibody incubations in the blocking buffer at room temperature for 2 h. Proteins were visualized with Amersham ECL Western Blotting Detection Reagent (GE), Clarity ECL Western Blotting Substrate (Bio-Rad) or SuperSignal West Femto Maximum Sensitivity Substrate (Thermo Scientific) and imaged using Image Lab software (Bio-Rad) on ChemiDoc XRS System (Bio-Rad).

Size-exclusion chromatography

Nuclear extracts were collected and diluted as described for immunoprecipitation. Lysates were incubated overnight at 4°C and centrifuged through a 0.45 μm Ultrafree-MC HV Centrifugal Filter (UFC30HVNB, EMD Millipore) before being applied to a pre-equilibrated Superose 6 10/300 GL column (17-5172-01, GE Healthcare Life Sciences). Fractions were collected and separated by SDS-PAGE on 4%–20% Tris-Glycine gels. The Superose 6 standard curve supplied by manufacturer was used to estimate molecular weight range for the collected fractions.

RNA extraction and quantitative PCR

Total RNA was extracted and purified from cells using the Quick-RNA MiniPrep Kit (Zymo Research, Irvine, CA). Equal amounts of RNA were reverse transcribed using High Capacity RNA to cDNA Kit (Applied Biosystems, Foster City, CA) according to the manufacturer's instructions. Real-time PCR reactions were prepared with PowerUp SYBR Green Master Mix (Applied Biosystems, Foster City, CA). mRNA levels were normalized to the house-keeping gene, β-actin.

Immunoprecipitation for mass spectrometry analyses

For AP-MS, cell extracts were pre-cleared with Protein-G Dynabeads for 1 h at 4°C before primary antibody incubation. For TAP-MS, whole cell extracts were incubated with Strep-Tactin Sepharose (IBA) at 4°C overnight. Cell extracts were washed three times in wash buffer and incubated in 1x Strep-tag elution buffer (IBA) for 10 min at room temperature on gentle vortex. The eluted solution was diluted with five times wash buffer and incubated with EZview red Flag M2 affinity gel (Sigma) for 4 h at 4°C. Beads were washed three times and eluted in wash buffer containing 150 μg/mL Flag peptide (Sigma) for 30 min at room temperature on gentle vortex.

Mass spectrometry

MS sample preparation and analyses were performed by the Stanford University Mass Spectrometry facility. In brief, for gel-free MS analysis, the final elutions from immunoprecipitations were solubilized and digested using the filter aided sample preparation (FASP) protocol (Wiśniewski et al., 2009). For gel-based analysis, final elutions were separated by 4%–20% SDS-PAGE (Bio-Rad) followed by silver staining (Thermo Scientific). Gel fragments were excised and cut into 1 mm^3 cubes, reduced with 5 mM DTT and alkylated with acrylamide. Trypsin/Lys-C Mix (Promega) was used as the protease for protein digestion. Peptides were extracted and dried using a speed-vac prior to reconstitution and analysis.

Nano reverse-phase HPLC was performed using either an Eksigent 2D nanoLC (Eksigent) or Waters nanoAcquity (Waters) with mobile phase A consisting of 0.1% formic acid in water and mobile phase B consisting of 0.1% formic acid in acetonitrile. A fused silica column self packed with duragel. C18 (Peeke) matrix was used with a linear gradient from 2% B to 40% B at a flow rate of 600 nL/minute. The nanoHPLC was interfaced with a Bruker/Michrom Advance Captive spray source for nanoESI into either a LTQ Orbitrap Velos mass spectrometer (Thermo Fisher Scientific) or an Orbitrap Elite (Thermo Fisher Scientific) operating in data-dependent acquisition mode to perform MS/MS on the top twelve most intense multiply charged cations.

Statistical analysis for AP-MS and TAP-MS

PPARγ AP-MS RAW data were searched with MaxQuant v. 1.5.0 (Cox and Mann, 2008) using default options, enabling matching between runs, against the reviewed version of the human reference proteome (07/30/2013). Then, the MS-1 peak intensities were

Log2-transformed and their distributions were median-centered across all runs. Missing intensities for peptides in a given run were imputed by setting their value to the mean minimal intensity across all runs, as an estimate for the under limit of detectability by MS. The normalized dataset was then analyzed by fitting a mixed effects model per protein in MSstats (v. 2.3.4, available on msstats.org) (Choi et al., 2014b) using the model without interaction terms, unequal feature variance and restricted scope of technical and biological replication. Pathway analyses were performed using COMPLEAT (Vinayagam et al., 2013) and Ingenuity Pathway Analysis (QIAGEN) and further curated manually based on published literature. Finally, known interactions between the 47 high confidence interactors of the DDR and replication pathway were computed by mining the COMPLEAT dataset and represented using Cytoscape (v.2.8.3) (Smoot et al., 2011).

For analysis of potential crosslinked peptides, data were searched using Byonic v3.1.0 (Protein Metrics), allowing for crosslinks between PPARγ and NBS1, assuming that peptides were tryptic with up to two missed cleavages and linked by BS3. The resulting spectral assignments were further analyzed using Byologic v3.2-38 (Protein Metrics) to identify and qualitatively assess crosslinked spectra at a chromatographic, MS1, and MS/MS level as described previously (https://www.ncbi.nlm.nih.gov/pubmed/28431242). Following this qualitative assessment, potential crosslinked peptides were compared against structural constraints based on the crystallography source PDB ID: 3DZU (Chandra et al., 2008) using the PyMOL Molecular Graphics System v.2.2.2 (Schrödinger, LLC).

EdU incorporation assay for cell cycle analysis

Cell cycle analysis was performed using the Click-iT EdU Alexa Fluor 647 Flow Cytometry Assay Kit (Thermo Fisher Scientific) according to the manufacturer's protocol. EdU (5-ethynyl-2′-deoxyuridine, 10 μM) was added to cells 2 h before harvest. Cells were co-stained with propidium iodide to quantitate DNA content.

Alkaline comet assay

DNA breaks were monitored using the CometAssay Reagent Kit for Single Cell Gel Electrophoresis Assay (Trevigen) according to the manufacturer's protocol. DNA was stained with SYBR-gold (Thermo Fisher Scientific). The comet tail lengths (defined as the length from the center of the DNA head to the end of the DNA tail) were measured by counting 100-150 cells for each sample and analyzed using ImageJ (v. 2.0) with a Comet Assay Plugin, downloaded from https://www.med.unc.edu/microscopy/resources/imagej-plugins-and-macros/comet-assay. The box in box-and-whiskers plots corresponds to the 25th to 75th percentiles. The line in the box marks the median and whiskers correspond to the 10th to 90th percentiles. Data points represent average comet tail length per sample. The outliers are represented as dots outside the whiskers.

Hypoxia and Reoxygenation

Cells were seeded on coverslips overnight and transferred to a Baker Ruskinn Concept anaerobic (< 0.1% O_2) chamber. Cells were incubated for 24 hours before exposing to room air for 10 min to induce oxidative damage. Cells were fixed according to the immunofluorescence protocol.

Immunofluorescence staining and confocal microscopy

After staining cultured cells, to avoid bias coverslips were randomly assigned with a number. The investigator was blinded to the randomization during data acquisition and analyses. Cultured cells were seeded on coverslips pre-coated with mouse Collagen IV (Corning). For staining of pATM (S1981), pRPA2 (S4/8), γH2AX and 8-oxo-dG foci, cells were pre-extracted with ice-cold 0.25% Triton in TBS at 4°C for 10 min with gentle rocking. Cells were then washed in TBS and fixed with 4% paraformaldehyde (Electron Microscopy Sciences) at room temperature for 10 min. After fixation, cells were blocked with 3% BSA in TBST at room temperature for 1 h. Primary antibody incubations were carried out in the blocking buffer at 4°C overnight, and secondary antibody incubations in the blocking buffer at room temperature for 1 h. Cells were mounted with DAPI Fluoromount-G (DAPI, 4,6-diamidino-2-phenylindole) (SouthernBiotech). Stained cells were imaged using Leica Application Suite X software on a Leica CTR 6500 (Leica).

For staining lung tissue sections, the genotypes of the lung sections were blinded to the investigator before the staining procedures were carried out, and during the data acquisition. Lungs tissues were fixed with 10% Neutral Buffered Formalin (Thermo Scientific) and embedded in paraffin (Leica). Sections were first deparaffinized and rehydrated. For antigen retrieval, sections were incubated in sub-boiling buffer (0.25 mM EDTA, pH 8.0) for 50 min. After cooling to room temperature, sections were incubated in 3% H_2O_2 for 10 min. Sections were incubated with the blocking buffer [3% normal goat serum (Jackson ImmunoResearch), 2% BSA, 0.2% Triton] at room temperature for 1 h. Primary antibody incubation was then carried out at 4°C overnight, followed by secondary antibody incubation at room temperature for 1 h. Sections were mounted with VECTASHIELD Antifade Mounting Medium with DAPI (Vector Laboratories). Stained lung sections were imaged using the FV10-ASW4.3 software on a Fluoview 1000 confocal microscope.

Immunofluorescence image analyses

For pATM (S1981), pPRA2 (S4/8), γH2AX and 8-oxo-dG imaging, 1-3 fields were acquired with the 20X objective to obtain 100-150 cells per sample. Nuclear fluorescence intensities were measured using ImageJ (Schneider et al., 2012), and box-and-whiskers graphs generated as described above. Each data point represents nuclear fluorescence per cell. Each graph is representative of one out of three independent experiments.

For evaluating γH2AX in mouse lung sections, 7 - 11 arteries (based on vWF staining and location) per animal (5 animals per group) were imaged. For evaluating γH2AX in clinical lung sections, 3 - 6 arteries (based on vWF staining and location) per subject were imaged (control: 6 and PAH: 5 subjects). Z stacked images were acquired with the 60X and 40X objectives for the mouse and human samples respectively. Nuclear γH2AX fluorescence was measured using the FociCounter software. The box-and-whiskers plots were generated as described above. Each data point represents average nuclear γH2AX fluorescence (after normalization to cell number) per artery. Details can be found in Supplemental Information.

QUANTIFICATION AND STATISTICAL ANALYSIS

Statistical analyses were performed using GraphPad Prism 6.0 (GraphPad Software). Experimental data were first subjected to the Shapiro-Wilk normality test to determine if the data are of a Gaussian distribution. The following tests were then selected for further statistical analyses. For pairwise comparison, unpaired t test (parametric) or two-tailed Mann-Whitney test (nonparametric) was used. For one-way ANOVA, Fisher's LSD test was used for pairwise comparison. For two-way ANOVA, Fisher's LSD test was used for pairwise comparison. For comparing immunofluorescence signals in more than two groups, Kruskal–Wallis ANOVA test followed by Dunn's test was used. P values are indicated as *, $p < 0.05$; **, $p < 0.01$; ***, $p < 0.001$; ****, $p < 0.0001$.

DATA AND SOFTWARE AVAILABILITY

The accession number for the mass spectrometry data generated from this study is Mass Spectrometry Interactive Virtual Environment (MassIVE) database: MSV000083257.

Cell Reports, Volume *26*

Supplemental Information

PPARγ Interaction with UBR5/ATMIN Promotes DNA Repair to Maintain Endothelial Homeostasis

Caiyun G. Li, Cathal Mahon, Nathaly M. Sweeney, Erik Verschueren, Vivek Kantamani, Dan Li, Jan K. Hennigs, David P. Marciano, Isabel Diebold, Ossama Abu-Halawa, Matthew Elliott, Silin Sa, Feng Guo, Lingli Wang, Aiqin Cao, Christophe Guignabert, Julie Sollier, Nils P. Nickel, Mark Kaschwich, Karlene A. Cimprich, and Marlene Rabinovitch

Supplementary Information

Figure S1

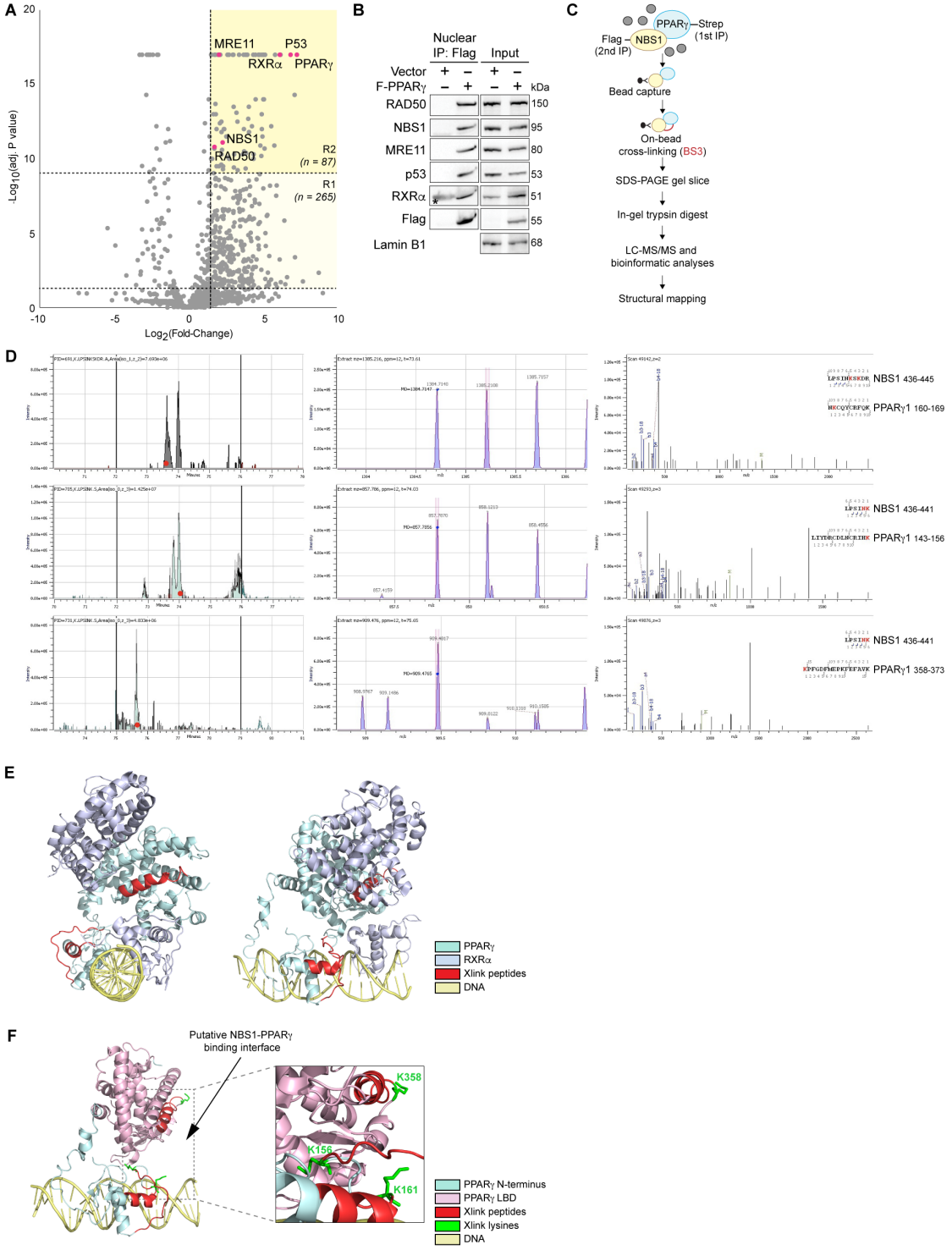

Figure S1 PPARγ interacts with the MRE11-RAD50-NBS1 (MRN) complex via NBS1 in 293T cells. – Related to Figure 1, Table S1-2.

(A) AP-MS experiments yielded a volcano plot revealing 87 PPARγ high confidence interactors (R2) out of the 352 interactors (R1+R2). Four (in red) were validated in (C) Dotted lines represent cut-off at Log_2(Fold-Change > 1.5) and Log_{10}(adj. P value ≤ 0.05 and $1.0x10^{-9}$). R1, region 1; R2, region 2, described in Results.

(B) Representative immunoblots of PPARγ interactions in 293T nuclear extracts.
(C) Experimental set up of the BS3 crosslinking mass spectrometry (XL-MS) using tandem immunoprecipitation of Flag-NBS1 and PPARγ-Strep to determine NBS1 and PPARγ binding interface.
(D) Raw MS/MS data of the identified crosslinked peptides from BS3 treated beads and trypsin-digested NBS1 and PPARγ. Amino acid positions of the peptides are as indicated. Analyses and methods are described in experimental procedures.
(E) Structural mapping of the three PPARγ peptides (red) identified in (D) to PPARγ crystal structure (light green) obtained from PDB:3DZU. This structure depicts PPARγ and RXRα (blue) complex on DNA (yellow).
(F) Putative NBS1-PPARγ binding interface as indicated by the locations of the three Xlink peptides (red). The Xlink lysines (K) are labeled as green in inset. PPARγ N-terminus is in light green, and its ligand-binding domain (LBD) is in pink.

Figure S2

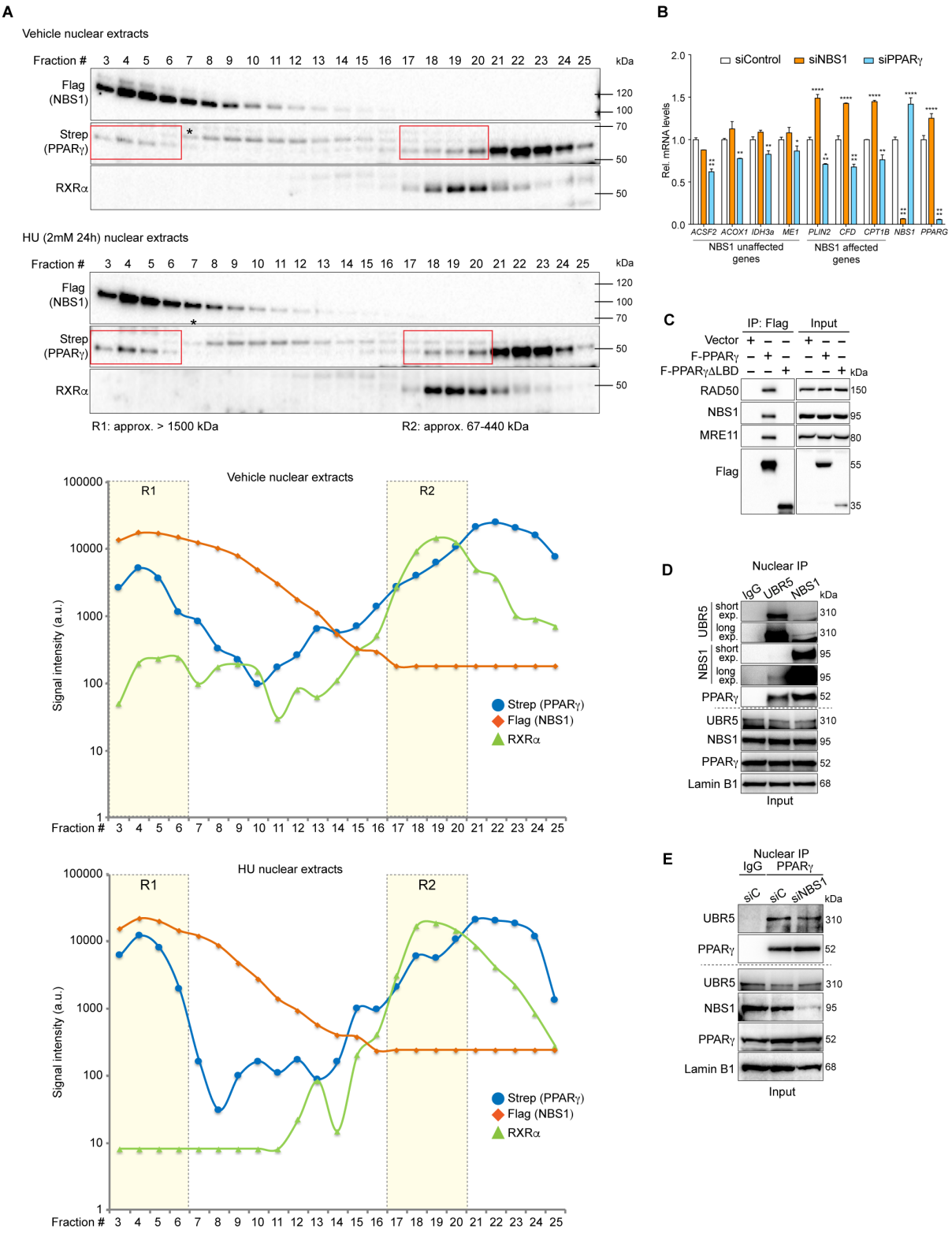

Figure S2 Nuclear PPARγ and NBS1 are in an independent cellular pool from PPARγ and RXRα. – Related to Figure 1.

(A) 293T nuclear extracts expressing PPARγ-2xStrep and Flag-NBS1 with and without HU treatment were analyzed by size-exclusion chromatography on a Superose 6 gel filtration column. Proteins eluted from fractions #3-25 were further analyzed by immunoblots to detect PPARγ (anti-Strep), NBS1 (ant-Flag) and RXRα (anti-RXRα). Graphs indicate densitometry results of each protein. Region 1 and 2 (R1, R2) are highlighted in red (in immunoblots) and yellow (in graphs) to indicate PPARγ eluted fractions. Since PPARγ-2xStrep is approximately (approx.) a 60 kDa protein (analyzed by silver staining in Fig. 1e), PPARγ eluted from fraction #21 (approx. 67 kDa) might be the excess monomeric form (due to overexpression). * indicates non-specific band.
(B) mRNA expression of PPARγ target genes with NBS1 or PPARγ depletion. mRNA expression was normalized to *β-actin* mRNA.
(C) Representative immunoblots of interactions between Flag-PPARγ (F-PPARγ) without the ligand binding domain (ΔLBD) and MRN.
(E) Representative immunoblots of endogenous co-immunoprecipitation (co-IP) between nuclear UBR5, NBS1 and PPARγ using anti-UBR5 or anti-NBS1.
(F) Representative immunoblots of endogenous IP of PPARγ with UBR5 with NBS1 depletion (siNBS1).
Error bars, mean ± s.e.m. (B). siC, siControl. Two-way ANOVA test with Fisher's LSD test (B). *, $P < 0.05$, **, $P < 0.01$, ***, $P < 0.001$, ****, $P < 0.0001$.

siC, siControl, siPγ, siPPARγ, siU5, siUBR5. Error bars, mean ± s.e.m. (B). siC, siControl. Two-way ANOVA test with Fisher's LSD test (A-C). One-way ANOVA test with Fisher's LSD test (G). *, $P < 0.05$, **, $P < 0.01$, ***, $P < 0.001$, ****, $P < 0.0001$.

Figure S3

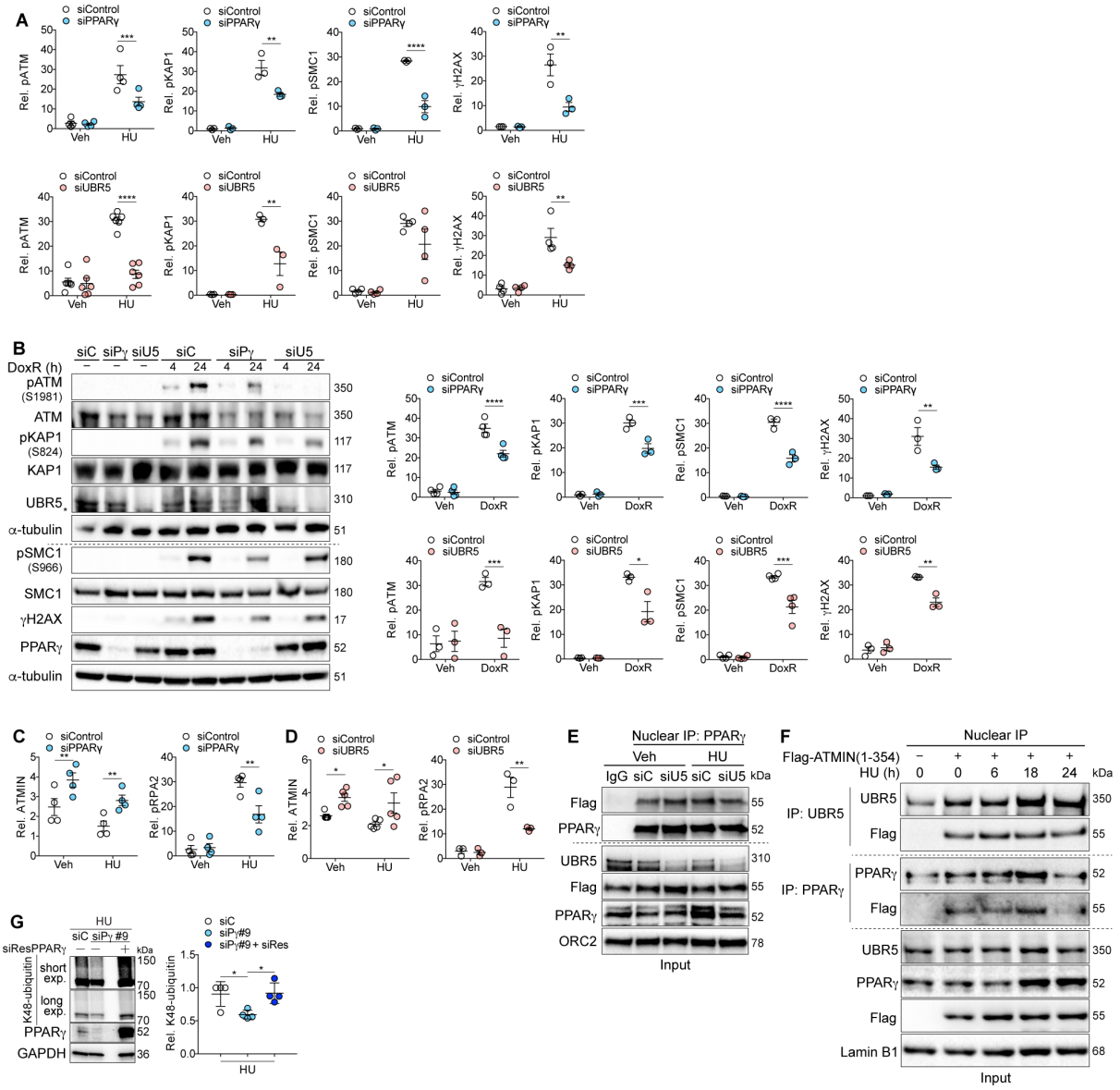

Figure S3 PPARγ promotes ATM signaling by increasing ATMIN ubiquitination in 293T cells. – Related to Figure 2.

(A) Densitometry of HU-induced ATM signaling pathways, pATM, pKAP1, pSMC1, γH2AX levels with PPARγ or UBR5 depletion.

(B) Representative immunoblots and densitometry data of DoxR-induced ATM signaling pathways, pATM, pKAP1, pSMC1, γH2AX levels with PPARγ or UBR5 depletions.

(C) Densitometry data of HU-induced ATMIN and pRPA2 with PPARγ depletion.

(D) Densitometry data of HU-induced ATMIN and pRPA2 with UBR5 depletion.

(E) Representative immunoblots of endogenous IP of nuclear PPARγ with Flag-ATMIN (aa1-354) with UBR5 depletion.

(F) Representative immunoblots of endogenous IP of nuclear PPARγ or UBR5 with Flag-ATMIN (aa1-354) with HU. The samples were harvested at the indicated time after HU treatment and lysates were separately incubated with anti-PPARγ or anti-UBR5.

(G) Representative immunoblots and densitometry data of restoration of K48-linked polyubiquitins with siRNA (siPPARγ#9)-resistant PPARγ overexpression.

Figure S4

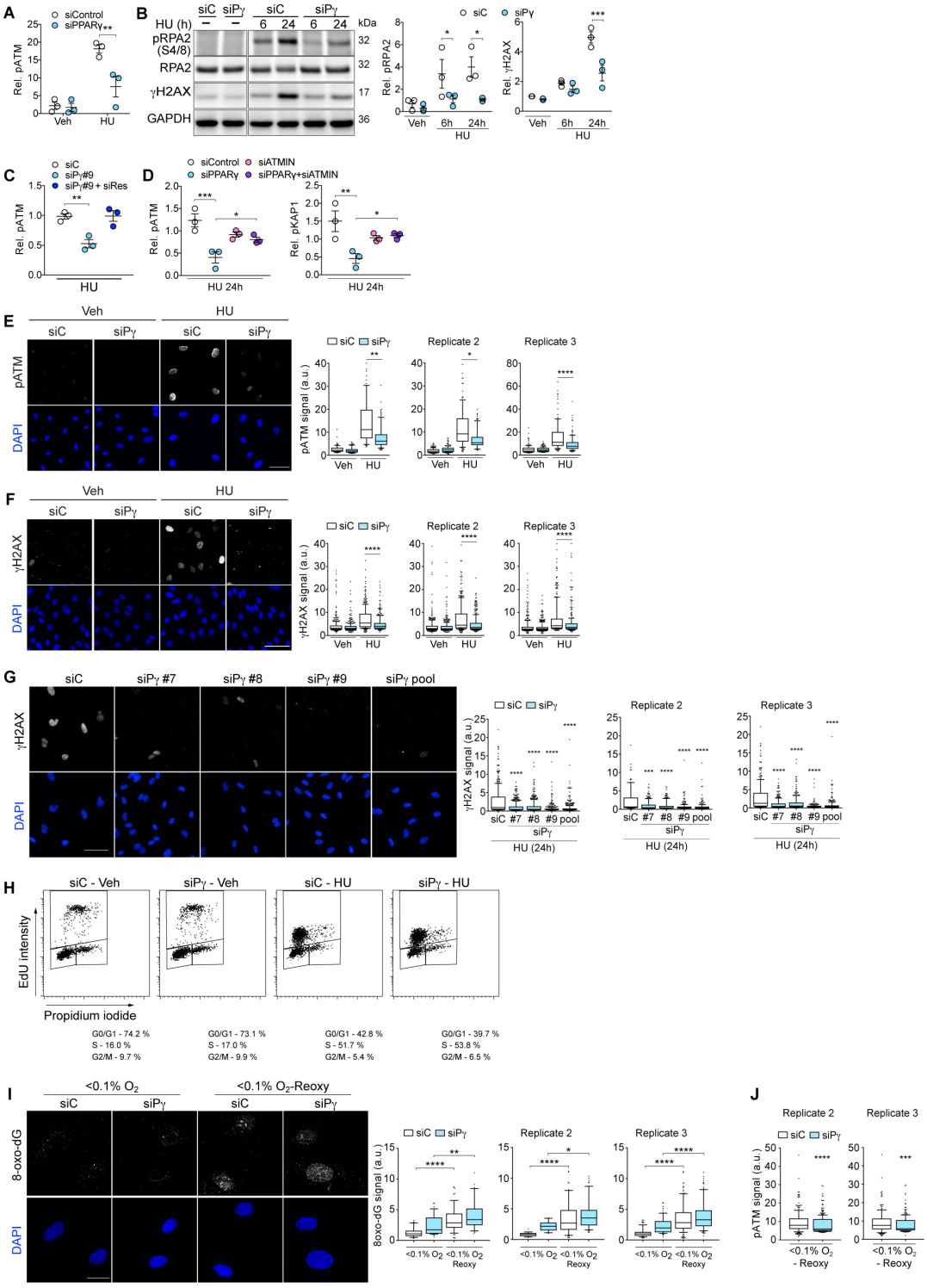

Fig. S4 PPARγ depletion suppresses pATM and γH2AX foci formation with various DNA damage stimuli and has no effects on cell cycle in primary endothelial cells. – Related to Figure 3.

(A) Densitometry data of HU-induced pATM with PPARγ depletion in PAEC.

(B) Representative immunoblots and densitometry data of HU-induced pRPA2 (S4/8) and γH2AX protein levels with PPARγ depletion in PAEC.

(C) Densitometry data of restoration of pATM with siRNA-resistant PPARγ (siResPPARγ) overexpression in HUVEC.
(D) Densitometry data of HU-induced pATM and pKAP1 with PPARγ or/and ATMIN depletion in PAEC.
(E) Confocal microscopy and triplicate quantitative data of effects of PPARγ depletion on pATM foci formation upon HU (24 hours) treatment in PAEC.
(F) Confocal microscopy and triplicate quantitative data of effects of PPARγ depletion on γH2AX foci formation upon HU (24 hours) treatment in PAEC.
(G) Confocal microscopy and triplicate quantitative data of effects of PPARγ depletion by multiple siRNAs on γH2AX foci formation upon HU (24 hours) treatment in PAEC. PPARγ siRNAs (#7-9) are three out of the four individual PPARγ siRNAs used in the siPγ pool.
(H) Flow cytometry analysis of EdU incorporation shows cell cycle profiles of cells with PPARγ depletion and with HU (24 hours) treatment in PAEC.
(I) Confocal microscopy and triplicate quantitative data of 8-oxo-dG foci upon hypoxia (24 hours) (< 0.1% O_2) and 10 min reoxygenation (Reoxy) in PAEC.
(J) Replicate quantitative data of pATM foci with hypoxia-reoxygenation as described in (I).
siC, siControl, siPγ, siPPARγ. Error bars, mean ± s.e.m. The line in the box-and-whisker plots marks the median and whiskers correspond to the 10^{th} to 90^{th} percentiles (E-G, I-J). Two-way ANOVA with Fisher's LSD test (A-D). Kruskal–Wallis ANOVA test with Dunn's test (E-G, I). Unpaired t test (J). *, $P < 0.05$, **, $P < 0.01$, ***, $P < 0.001$; ****, $P < 0.0001$. Scale bars, E-G, 50μm; I, 20μm.

Figure S5

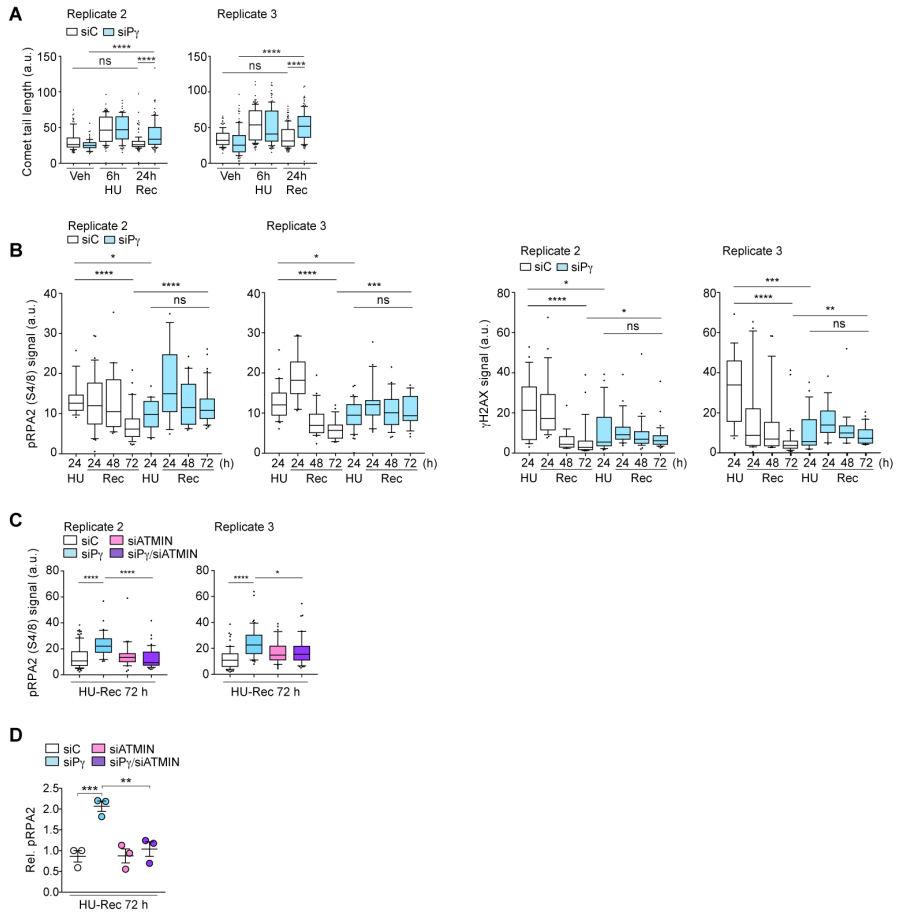

Fig. S5 PPARγ depletion leads to persistent pRPA2 and γH2AX foci after HU-induced damage which are resolved by ATMIN depletion in PAEC. – Related to Figure 4.

(A) Replicate quantitative data of extended comet tail lengths in PPARγ depleted cells after HU (6 hours) was removed (recovery for 24 hours).

(B) Replicate quantitative data of pRPA2 and γH2AX foci in PPARγ depleted cells after HU (24 hours) was removed. Cells were fixed at various recovery time points as indicated.

(C) Replicate quantitative data of resolution of pRPA2 foci with ATMIN depletion in addition to PPARγ depletion.

(D) Densitometry data show restoration of pRPA2 protein levels with ATMIN depletion in addition to PPARγ depletion.

siC, siControl, siPγ, siPPARγ. Error bars, mean ± s.e.m. The line in the box-and-whisker plots marks the median and whiskers correspond to the 10th to 90th percentiles (A-C). Kruskal–Wallis ANOVA test with Dunn's test (A-C). Two-way ANOVA with Fisher's LSD test (D). *, $P < 0.05$, **, $P < 0.01$, ***, $P < 0.001$; ****, $P < 0.0001$, ns, not significant.

Figure S6

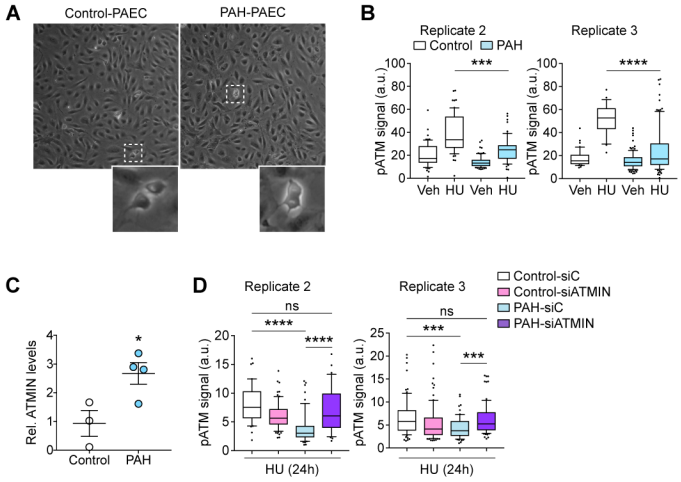

Fig. S6 PPARγ and ATMIN axis is impaired in PAEC from PAH patients. – Related to Figure 5.
(A) Phase-contrast microscopy shows healthy primary PAEC cultures established from explanted lungs of control (unused donors) and PAH patient. Inserts indicate mitotic cells from the dotted square.
(B) Replicate quantitative data of HU-induced pATM levels in control and PAH-PAEC.
(C) Densitometry data of ATMIN protein levels in control and PAH-PAEC.
(D) Replicate quantitative data of pATM levels in control and PAH-PAEC with ATMIN depletion.
siC, siControl, siPγ, siPPARγ. Error bars, mean ± s.e.m. The line in the box-and-whisker plots marks the median and whiskers correspond to the 10^{th} to 90^{th} percentiles (B,D). Kruskal–Wallis ANOVA test with Dunn's test (B,D). Unpaired t test (C). *, $P < 0.05$, ***, $P < 0.001$; ****, $P < 0.0001$, ns, not significant.

121 **Table S1 High-confidence PPARγ interactors identified from AP-MS. – Related to Figure 1; Figure S1.**

Uniprot ID	Log2FC	Adj. P value	Gene name	Protein name
P37231	7.32	0	PPARG	Peroxisome proliferator-activated receptor gamma
P04637	6.9	0	TP53	Cellular tumor antigen p53
P11142	6.22	0	HSPA8	Heat shock cognate 71 kDa protein
O95816	6.22	0	BAG2	BAG family molecular chaperone regulator 2
P19793	6.17	0	RXRA	Retinoic acid receptor RXR-alpha
P23396	5.86	0	RPS3	40S ribosomal protein S3
P52272	5.18	0	HNRNPM	Heterogeneous nuclear ribonucleoprotein M
P31943	5.08	0	HNRNPH1	Heterogeneous nuclear ribonucleoprotein H, N-terminally processed
P49411	4.97	0	TUFM	Elongation factor Tu, mitochondrial
P49368	4.82	0	CCT3	T-complex protein 1 subunit gamma
Q92841	4.74	0	DDX17	Probable ATP-dependent RNA helicase DDX17
P08107	4.53	0	HSPA1B	Heat shock 70 kDa protein 1A/1B
P17987	4.38	0	TCP1	T-complex protein 1 subunit alpha
P55072	3.98	0	VCP	Transitional endoplasmic reticulum ATPase
Q9UL15	3.91	0	BAG5	BAG family molecular chaperone regulator 5
Q08211	3.87	0	DHX9	ATP-dependent RNA helicase A
P18669	3.74	0	PGAM1	Phosphoglycerate mutase 1
P48047	3.43	0	ATP5O	ATP synthase subunit O, mitochondrial
P52209	3.43	0	PGD	6-phosphogluconate dehydrogenase, decarboxylating
Q9Y265	3.05	0	RUVBL1	RuvB-like 1
Q9Y230	3.03	0	RUVBL2	RuvB-like 2
P38646	3	0	HSPA9	Stress-70 protein, mitochondrial
P11021	2.74	0	HSPA5	78 kDa glucose-regulated protein
P13796	2.65	0	LCP1	Plastin-2
P50990	2.65	0	CCT8	T-complex protein 1 subunit theta
O14830	2.16	0	PPEF2	Serine/threonine-protein phosphatase with EF-hands 2
P47929	2.11	0	LGALS7	Galectin-7
P49959	2.08	0	MRE11A	Meiotic recombination 11 MRE11A
Q02880	2	0	TOP2B	DNA topoisomerase 2-beta
Q9H0A0	1.83	0	NAT10	N-acetyltransferase 10
Q9Y490	1.79	0	TLN1	Talin-1
P15927	1.58	0	RPA2	Replication protein A 32 kDa subunit
P49916	1.55	0	LIG3	DNA ligase 3
Q9UBQ0	1.54	0	VPS29	Vacuolar protein sorting-associated protein 29
P62241	7.17	5.57E-15	RPS8	40S ribosomal protein S8
Q86U86	5.1	1.02E-14	PBRM1	Protein polybromo-1
Q7Z2W4	5.06	1.02E-14	ZC3HAV1	Zinc finger CCCH-type antiviral protein 1
Q92945	4.55	1.02E-14	KHSRP	Far upstream element-binding protein 2
Q6Y7W6	1.83	2.01E-14	GIGYF2	PERQ amino acid-rich with GYF domain-containing protein 2
P33993	4.09	2.95E-14	MCM7	DNA replication licensing factor MCM7
P17066	3.06	3.37E-14	HSPA6	Heat shock 70 kDa protein 6
Q13263	3.26	8.51E-14	TRIM28	Transcription intermediary factor 1-beta
Q9H583	1.86	1.02E-13	HEATR1	HEAT repeat-containing protein 1, N-terminally processed
P42704	1.71	1.05E-13	LRPPRC	Leucine-rich PPR motif-containing protein, mitochondrial
P62906	4.96	1.07E-13	RPL10A	60S ribosomal protein L10a
Q14151	4.04	2.02E-13	SAFB2	Scaffold attachment factor B2
Q15393	3.32	3.40E-13	SF3B3	Splicing factor 3B subunit 3
P78316	2.24	3.40E-13	NOP14	Nucleolar protein 14
P62424	2.14	3.78E-13	RPL7A	60S ribosomal protein L7a

P32969	5.6	6.05E-13	RPL9P7	60S ribosomal protein L9
P78347	4.3	6.89E-13	GTF2I	General transcription factor II-I
Q99615	4.96	9.02E-13	DNAJC7	DnaJ homolog subfamily C member 7
Q15029	3.75	9.05E-13	EFTUD2	116 kDa U5 small nuclear ribonucleoprotein component
Q9NVP1	2.43	9.05E-13	DDX18	ATP-dependent RNA helicase DDX18
O75368	1.91	1.10E-12	SH3BGRL	SH3 domain-binding glutamic acid-rich-like protein
O95786	2.4	1.11E-12	DDX58	Probable ATP-dependent RNA helicase DDX58
P28702	4.1	1.50E-12	RXRB	Retinoic acid receptor RXR-beta
P61978	2.25	1.66E-12	HNRNPK	Heterogeneous nuclear ribonucleoprotein K
Q96EY1	5.01	2.90E-12	DNAJA3	DnaJ homolog subfamily A member 3, mitochondrial
Q8N1F7	2.57	3.12E-12	NUP93	Nuclear pore complex protein Nup93
O60934	2.32	8.83E-12	NBS1	Nibrin
O00231	4.86	1.18E-11	PSMD11	26S proteasome non-ATPase regulatory subunit 11
Q12906	5.8	1.22E-11	ILF3	Interleukin enhancer-binding factor 3
Q92878	1.77	1.47E-11	RAD50	DNA repair protein RAD50
O60264	1.76	2.00E-11	SMARCA5	SWI/SNF-related matrix-associated actin-dependent regulator of chromatin subfamily A member 5
O15042	5.15	2.02E-11	U2SURP	U2 snRNP-associated SURP motif-containing protein
O76021	2.28	2.53E-11	RSL1D1	Ribosomal L1 domain-containing protein 1
P62191	3.77	3.35E-11	PSMC1	26S protease regulatory subunit 4
P46087	3.91	3.67E-11	NOP2	Probable 28S rRNA (cytosine(4447)-C(5))-methyltransferase
Q9Y2R4	3.68	4.88E-11	DDX52	Probable ATP-dependent RNA helicase DDX52
Q9BVJ6	4.41	4.97E-11	UTP14A	U3 small nucleolar RNA-associated protein 14 homolog A
O15144	2.26	5.08E-11	ARPC2	Actin-related protein 2/3 complex subunit 2
Q12905	3.1	5.40E-11	ILF2	Interleukin enhancer-binding factor 2
P62701	4.93	5.77E-11	RPS4X	40S ribosomal protein S4, X isoform
Q9BZE4	2.7	7.08E-11	GTPBP4	Nucleolar GTP-binding protein 1
O75367	2.76	9.21E-11	H2AFY	Core histone macro-H2A.1
P15924	1.62	9.21E-11	DSP	Desmoplakin
Q9Y2X3	4.4	9.27E-11	NOP58	Nucleolar protein 58
Q8WVV4	1.54	1.01E-10	POF1B	Protein POF1B
P17931	2.23	2.46E-10	LGALS3	Galectin-3
Q9BVP2	2.07	3.14E-10	GNL3	Guanine nucleotide-binding protein-like 3
P26038	2.36	3.16E-10	MSN	Moesin
P06702	1.91	3.16E-10	S100A9	Protein S100-A9
P07900	3.08	3.80E-10	HSP90AA1	Heat shock protein HSP 90-alpha
P31689	3.87	4.49E-10	DNAJA1	DnaJ homolog subfamily A member 1
O15511	2.34	5.01E-10	ARPC5	Actin-related protein 2/3 complex subunit 5
O15160	3.33	5.70E-10	POLR1C	DNA-directed RNA polymerases I and III subunit RPAC1
O43818	1.72	9.22E-10	RRP9	U3 small nucleolar RNA-interacting protein 2

Proteins co-purified with Flag-PPARγ from 293T nuclear extracts were detected by mass spectrometry and analyzed as described in Experimental Procedures. Proteins in red were validated in Fig. 1c. Log_2FC (Fold-Change) indicates the fold enrichment of proteins immunoprecipitated from Flag-PPARγ expressing cells as compared to Flag-vector expressing cells. The adjusted (adj.) P values are indicated and the data was obtained from four independent experiments. Proteins are listed by their adj. P values.

Table S2

Biological functions associated with the high-confidence PPARγ interactome. – Related to Figure 1; Figure S1.

Uniprot ID	Gene name	Biological function name
O15144	ARPC2	Actin cytoskeleton organization
O15511	ARPC5	Actin cytoskeleton organization
P47929	LGALS7	Cell-cell interaction
Q8WVV4	POF1B	Cell-cell interaction
Q9Y490	TLN1	Cell-cell interaction
P48047	ATP5O	Cellular metabolism
O95816	BAG2	Cellular metabolism
Q9UL15	BAG5	Cellular metabolism
P18669	PGAM1	Cellular metabolism
P52209	PGD	Cellular metabolism
P37231	PPARG	Cellular metabolism
P19793	RXRA	Cellular metabolism
P28702	RXRB	Cellular metabolism
P49411	TUFM	Cellular metabolism
Q9UBQ0	VPS29	Cellular metabolism
Q08211	DHX9	DNA damage response and replication
P31689	DNAJA1	DNA damage response and replication
Q96EY1	DNAJA3	DNA damage response and replication
O75367	H2AFY	DNA damage response and replication
P07900	HSP90AA1	DNA damage response and replication
P08107	HSPA1B	DNA damage response and replication
P11142	HSPA8	DNA damage response and replication
Q92945	KHSRP	DNA damage response and replication
P49916	LIG3	DNA damage response and replication
P42704	LRPPRC	DNA damage response and replication
P33993	MCM7	DNA damage response and replication
P49959	MRE11A	DNA damage response and replication
O60934	NBN	DNA damage response and replication
Q8N1F7	NUP93	DNA damage response and replication
Q86U86	PBRM1	DNA damage response and replication
P62191	PSMC1	DNA damage response and replication
O00231	PSMD11	DNA damage response and replication
Q92878	RAD50	DNA damage response and replication
P15927	RPA2	DNA damage response and replication
Q9Y265	RUVBL1	DNA damage response and replication
Q9Y230	RUVBL2	DNA damage response and replication
Q14151	SAFB2	DNA damage response and replication
O60264	SMARCA5	DNA damage response and replication
Q02880	TOP2B	DNA damage response and replication
P04637	TP53	DNA damage response and replication
Q13263	TRIM28	DNA damage response and replication
P55072	VCP	DNA damage response and replication
O95786	DDX58	Innate immune response
P13796	LCP1	Innate immune response
P17931	LGALS3	Innate immune response
P06702	S100A9	Innate immune response
Q7Z2W4	ZC3HAV1	Innate immune response
Q92841	DDX17	mRNA metabolic process and RNA processing
Q9NVP1	DDX18	mRNA metabolic process and RNA processing
Q9Y2R4	DDX52	mRNA metabolic process and RNA processing

Q15029	EFTUD2	mRNA metabolic process and RNA processing
Q6Y7W6	GIGYF2	mRNA metabolic process and RNA processing
Q9BVP2	GNL3	mRNA metabolic process and RNA processing
Q9BZE4	GTPBP4	mRNA metabolic process and RNA processing
Q9H583	HEATR1	mRNA metabolic process and RNA processing
P31943	HNRNPH1	mRNA metabolic process and RNA processing
P61978	HNRNPK	mRNA metabolic process and RNA processing
P52272	HNRNPM	mRNA metabolic process and RNA processing
Q12905	ILF2	mRNA metabolic process and RNA processing
Q12906	ILF3	mRNA metabolic process and RNA processing
Q9H0A0	NAT10	mRNA metabolic process and RNA processing
P78316	NOP14	mRNA metabolic process and RNA processing
P46087	NOP2	mRNA metabolic process and RNA processing
Q9Y2X3	NOP58	mRNA metabolic process and RNA processing
P62906	RPL10A	mRNA metabolic process and RNA processing
P62424	RPL7A	mRNA metabolic process and RNA processing
P32969	RPL9P7	mRNA metabolic process and RNA processing
P23396	RPS3	mRNA metabolic process and RNA processing
P62701	RPS4X	mRNA metabolic process and RNA processing
P62241	RPS8	mRNA metabolic process and RNA processing
O43818	RRP9	mRNA metabolic process and RNA processing
O76021	RSL1D1	mRNA metabolic process and RNA processing
Q15393	SF3B3	mRNA metabolic process and RNA processing
O15042	U2SURP	mRNA metabolic process and RNA processing
Q9BVJ6	UTP14A	mRNA metabolic process and RNA processing
P49368	CCT3	Protein folding
P50990	CCT8	Protein folding
Q99615	DNAJC7	Protein folding
P15924	DSP	Protein folding
P11021	HSPA5	Protein folding
P17066	HSPA6	Protein folding
P38646	HSPA9	Protein folding
P26038	MSN	Protein folding
P17987	TCP1	Protein folding
P78347	GTF2I	NA
O15160	POLR1C	NA
O14830	PPEF2	NA
O75368	SH3BGRL	NA

Biological functions enriched among the top ranked 87 PPARγ interactors defined in Supplementary Table 1. NA, not available.

Table S3

Tandem affinity purification identified proteins interacting with PPARγ and NBS1 in unperturbed cells. – Related to Figure 1.

Uniprot ID	Log2FC	Adj. P value	Gene name	Protein name
O60934	6.24	0	NBS1	Nibrin
P37231	6.03	0	PPARG	Peroxisome proliferator-activated receptor gamma
P49959	5.22	0	MRE11A	Meiotic recombination 11 MRE11A
Q92878	5.01	0	RAD50	DNA repair protein RAD50
O95816	3.7	1.71E-08	BAG2	BAG family molecular chaperone regulator 2
Q9UL15	2.9	4.03E-07	BAG5	BAG family molecular chaperone regulator 5
O75594	2.56	2.25E-02	PGLYRP1	Peptidoglycan recognition protein 1
P04637	2.46	7.99E-09	TP53	Cellular tumor antigen p53
P62269	2.2	0	RPS18	40S ribosomal protein S18
Q07021	2.1	2.05E-08	C1QBP	Complement component 1 Q subcomponent-binding protein, mitochondrial
P23588	1.96	4.10E-10	EIF4B	Eukaryotic translation initiation factor 4B
Q02878	1.93	0	RPL6	60S ribosomal protein L6
P18124	1.9	1.60E-13	RPL7	60S ribosomal protein L7
P34932	1.84	0	HSPA4	Heat shock 70 kDa protein 4
P50914	1.8	0	RPL14	60S ribosomal protein L14
O95071	1.8	3.37E-02	UBR5*	E3 ubiquitin-protein ligase UBR5
P98175	1.78	4.19E-11	RBM10	RNA-binding protein 10
P62701	1.66	7.94E-07	RPS4X	40S ribosomal protein S4, X isoform
P62333	1.65	2.25E-03	PSMC6*	26S protease regulatory subunit 10B
Q9Y2W1	1.55	7.34E-11	THRAP3*	Thyroid hormone receptor-associated protein 3
P11142	1.54	0	HSPA8	Heat shock cognate 71 kDa protein

Proteins were co-purified with PPARγ-2xStrep and sequentially with Flag-NBS1 from 293T whole cell extracts [unperturbed cells or with HU treatment (Supplementary Table 4)]. Log_2FC indicates the fold enrichment of proteins immunoprecipitated from the PPARγ-2xStrep and Flag-NBS1 expressing cells as compared to GFP-Strep-Flag expressing cells (negative control). The adjusted P value is indicated and the data were obtained from three independent experiments.

* indicates proteins specifically enriched in unperturbed cells but not present in the HU treated cells. THRAP3 and UBR5 (red) are validated in Fig. 1e, f. Proteins are listed by the Log_2FC.

Table S4

Tandem affinity purification identified proteins interacting with PPARγ and NBS1 upon HU treatment. – Related to Figure 1.

Uniprot ID	Log2FC	Adj. P value	Gene name	Protein name
O60934	6.25	0	NBS1	Nibrin
P37231	6.09	0	PPARG	Peroxisome proliferator-activated receptor gamma
P49959	5.02	0	MRE11A	Meiotic recombination 11 MRE11A
Q92878	4.78	0	RAD50	DNA repair protein RAD50
O95816	3.88	6.05E-09	BAG2	BAG family molecular chaperone regulator 2
Q9UL15	3.65	7.27E-08	BAG5	BAG family molecular chaperone regulator 5
Q92552	3.16	3.37E-02	MRPS27*	28S ribosomal protein S27, mitochondrial
O75594	2.7	2.17E-02	PGLYRP1	Peptidoglycan recognition protein 1
Q02878	2.61	0	RPL6	60S ribosomal protein L6
P18124	2.58	0	RPL7	60S ribosomal protein L7
Q07021	2.36	1.18E-09	C1QBP	Complement component 1 Q subcomponent-binding protein, mitochondrial
P04637	2.08	6.15E-07	TP53	Cellular tumor antigen p53
P50914	2.07	0	RPL14	60S ribosomal protein L14
P43686	1.89	1.08E-07	PSMC4*	26S protease regulatory subunit 6B
Q9BRT6	1.87	4.32E-02	LLPH*	Protein LLP homolog
O60318	1.83	2.30E-02	MCM3AP*	Germinal-center associated nuclear protein
P11388	1.82	3.49E-09	TOP2A*	DNA topoisomerase 2-alpha
P23588	1.79	1.21E-09	EIF4B	Eukaryotic translation initiation factor 4B
P62269	1.78	0	RPS18	40S ribosomal protein S18
P98175	1.76	1.56E-11	RBM10	RNA-binding protein 10
Q75N03	1.73	1.62E-02	CBLL1*	E3 ubiquitin-protein ligase Hakai
P40429	1.71	2.38E-02	RPL13A*	60S ribosomal protein L13a
Q02880	1.7	3.50E-04	TOP2B*	DNA topoisomerase 2-beta
P36578	1.69	9.59E-14	RPL4*	60S ribosomal protein L4
Q9HAN9	1.67	3.64E-04	NMNAT1*	Nicotinamide/nicotinic acid mononucleotide adenylyltransferase 1
P62917	1.65	0	RPL8*	60S ribosomal protein L8
Q07020	1.64	6.87E-10	RPL18*	60S ribosomal protein L18
P62266	1.62	6.37E-07	RPS23*	40S ribosomal protein S23
P62847	1.61	3.98E-09	RPS24*	40S ribosomal protein S24
P34932	1.61	8.63E-14	HSPA4	Heat shock 70 kDa protein 4
P62701	1.59	9.46E-07	RPS4X	40S ribosomal protein S4, X isoform
P11142	1.58	0	HSPA8	Heat shock cognate 71 kDa protein
P62158	1.56	2.83E-06	CALM2*	Calmodulin
P62249	1.55	5.53E-09	RPS16*	40S ribosomal protein S16
P62241	1.54	1.43E-08	RPS8*	40S ribosomal protein S8
P49368	1.51	2.20E-02	CCT3*	T-complex protein 1 subunit gamma

Proteins were co-purified with PPARγ-2xStrep and sequentially with Flag-NBS1 from 293T whole cell extracts with HU treatment. Log_2FC (Fold-Change) indicates the fold enrichment of proteins immunoprecipitated from the PPARγ-2xStrep and Flag-NBS1 expressing cells as compared to GFP-Strep-Flag expressing cells (negative control). The adjusted P value is indicated and the data were obtained from three independent experiments. * indicates proteins specifically enriched in the HU treated cells but not present in unperturbed cells. Proteins are listed by the Log_2FC.

Table S5 – Related to STAR Methods.
Characteristics of (a) control subjects and (b) PAH patients used in this study.
(a) Control

Control ID	Cells/ Tissues	Assays	Age (yr)/ Gender	Race/ Ethnicity	Cause of Death
Control-1	Tissue	IF	41/F	White/ Non-Hispanic	Grade 4 subarachnoid hemorrhage, ruptured anterior cerebral artery aneurysm
Control-2	Tissue	IF	43/M	White/ Non-Hispanic	Fatal gunshot to head
Control-3	Tissue	IF	57/F	White/ Non-Hispanic	Intracranial hemorrhage/stroke
Control-4	Tissue	IF	28/F	White/ Non-Hispanic	MVC-anoxia
Control-5	SPAEC	Comet	47/M	White/ Non-Hispanic	Head trauma-bicycle vs. car accident
Control-6	Tissue	IF	56/F	White/ Non-Hispanic	Cerebrovascular accident
Control-7	SPAEC	Comet	55/F	Unknown/ Hispanic or Latino	Cerebrovascular stroke
Control-8	Tissue/ LPAEC	IF, comet, protein expression	57-F	White/ Non-Hispanic	Acute myocardial infarction
Control-9	LPAEC	Comet	12/M	Unknown/ Non-Hispanic	Head trauma rollover MVC ejection
Control-10	LPAEC	Comet	49/M	White/ Non-Hispanic	Head trauma
Control-11	SPAEC	Protein expression	33/F	White/ Non-Hispanic	Head trauma. Blunt injury.

Control-12	LPAEC	IP, protein expression	54/M	Unknown/ Hispanic or Latino	Cerebrovascular/stroke ICH
Control-13	LPAEC	IP, protein expression	34/F	Asian/ Non-Hispanic	Cerebrovascular/stroke ICH
Control-14	LPAEC	IP	1/M	White/ Non-Hispanic	Anoxia/drowning
Control-15*	LPAEC	IP, protein expression	35/M	White/ Non-Hispanic	Gunshot wound
Control-16	LPAEC	IP, protein expression	46/M	Asian/Unknown	Cerebrovascular/stroke ICH

159

160 (b) PAH patients

Patient ID	**Cells/ Tissues**	**Assays**	**Age (yr)/ Gender**	**Race/ Ethnicity**	**Diagnosis**	**BMPR2 mutation**	**(s/d/m)PAPa**	**PVRb (mmHg)**	**6 Min Walkc (Wood Units)**	**PAH Medications (m), up to transplant date**
PAH-1	Tissue	IF	15-F	White/ Non-Hispanic	IPAH	No	(175/66/102)	25.24	387	sildenafil, epoprostenol
PAH-2	Tissue	IF	40-F	White/ Non-Hispanic	IPAH	No	(84/26/47)	NA	294	ambrisentan, sildenafil, iloprost, epoprostenol
PAH-3	LPAEC	Protein expressoo pm	33-F	Black or African American/ Non-Hispanic	FPAH	Yes	(75/33/48)	15.57	326.1	epoprostenol, bosentan, sildenafil, treprostinil
PAH-4	Tissue	IF	56-F	White/ Non-Hispanic	IPAH	No	(83/39/57)	11.41	137.2	sildenafil, ambrisentan, treprostinil
PAH-5	Tissue,S/ LPAEC	IF, comet,	27-F	White/ Non-Hispanic	IPAH	Yes	(110/49/69)	12.11	359.7	sildenafil, treprostinil, bosentan, iloprost

PAH-6	SPAEC	Comet	40-M	White/ Hispanic or Latino	IPAH	No	(118/49/64)	73	420	sildenafil, ambrisentan, treprostinil
PAH-7	SPAEC	Comet	37-M	White/ Non-Hispanic	FPAH	Yes	(119/51/77)	14.22	309	sildenafil, sitaxsentan, ambrisentan, epoprostenol, imatinib (investigational), treprostinil
PAH-8	LPAEC	Comet, IP, protein expression	32-F	White/ Non-Hispanic	IPAH	No	(68/38/49)	15.34	238	bosentan, epoprostenol
PAH-9	Tissue/ LPAEC	IF, comet, IP, protein expression	30-M	White/ Non-Hispanic	APAH-Congenital ASD	No	(128/60/85)	NA	160	sildenafil, bosentan
PAH-10	LPAEC	IP, protein expression	16-F	White/ Non-Hispanic	IPAH	N/A	(NA/NA/95)	N/A	102.4	sildenafil, subcutaneous treprostinil
PAH-11	LPAEC	Protein expression	50-F	White/ Hispanic or Latino	APAH-D&T	N/A	(113/43/65)	16.18	384	sildenafil, ambrisentan, bosentan, treprostinil, epoprostenol
PAH-12	LPAEC	Protein expression	22-F	White/ Non-Hispanic	FPAH	Yes	(98/46/66)	10.19	506	sildenafil, ambrisentan, tadalafil, treprostinil

a (s/d/m) PAP= Systolic, diastolic, and mean pulmonary arterial pressure. b PVR= Pulmonary vascular resistance. c 6 min walk = distance walked in six minutes.
a-c Values are closest to transplant date. * Control line that did not meet PHBI inclusion criteria due to known history of amphetamine/methamphetamine use.
Abbreviations: SPAEC, small pulmonary arterial endothelial cells (<1 mm by dissection); LPAEC, large PAEC (>1 mm); IF, immunofluorescence; IP, immunoprecipitation; F, female; M, male; MVC, motor vehicle accident; ICH, intracranial hemorrhage; IPAH, idiopathic pulmonary arterial hypertension; FPAH, familiar PAH; APAH, associated PAH; ASD, atrial septal defect ; D&T, drug and toxin; NA, not available.

Table S6 – Related to STAR Methods.
Table of Oligonucleotides used.

Oligo	Sequence (5'-3')	Description
PPARγ-delLBD_F	GTGGCCATCCGCATCTGACAGGGCTGCCAGTTTCG	Primer used for generating Flag-PPARγΔLBD
PPARγ-delLBD_R	CGAAACTGGCAGCCCTGTCAGATGCGGATGGCCAC	Primer used for generating Flag-PPARγΔLBD
2Strep-PPARγ-F	TAGTCCAGTGTGGTGGAATTCGCCGCCATGACCATGGTTGACACAG	Primer used for generating 2xStrep-PPARγ
2Strep-PPARγ-R	CACCGCCTCCCTCGAGCGGCCGCACGTACAAGTCCTTGTAG	Primer used for generating 2xStrep-PPARγ
siRES-PPARγ_F	ATGACAGCGATCTCGCAATATTTATTGCTGTCATTATTC	Primer used for generating siRNA-resistant-Flag-PPARγ
siRES-PPARγ_R	TAAATATTGCGAGATCGCTGTCATCTAATTCCAGTG	Primer used for generating siRNA-resistant-Flag-PPARγ
PPARγ_F	GCCGTGGCCGCAGATTTGAAAGA	Primer used for quantitative real-time PCR
PPARγ_R	TACGGAGAGATCCACGGAGCTGA	Primer used for quantitative real-time PCR
UBR5_F	CCTGCTCACTGCTACTAATCTG	Primer used for quantitative real-time PCR
UBR5_R	ATTCGAGGTGGCCTGTATTG	Primer used for quantitative real-time PCR
ATMIN_F	AACAGCACTGCAGTCTCACA	Primer used for quantitative real-time PCR
ATMIN_R	CTGGTCTAGGGATTGGTTGGT	Primer used for quantitative real-time PCR
NBS1_F	CACTCACCTTGTCATGGTATCAG	Primer used for quantitative real-time PCR
NBS1_R	CTGCTTCTTGGACTCAA CTGC	Primer used for quantitative real-time PCR
PLIN2_F	ATGGCATCCGTTGCAGTTGAT	Primer used for quantitative real-time PCR
PLIN2_R	GGACATGAGGTCATACGTGGAG	Primer used for quantitative real-time PCR
ACOX1_F	GGAACTCACCTTCGAGGCTTG	Primer used for quantitative real-time PCR
ACOX1_R	TTCCCCTTAGTGATGAGCTGG	Primer used for quantitative real-time PCR
CPT1B_F	CCTGCTACATGGCAACTGCTA	Primer used for quantitative real-time PCR
CPT1B_R	AGAGGTGCCCAATGATGGGA	Primer used for quantitative real-time PCR
ACSF2_F	ATGGCTGTCTACGTCGGG	Primer used for quantitative real-time PCR
ACSF2_R	GACCATGCGATCCACCTCTC	Primer used for quantitative real-time PCR
ME1_F	CTGCTGACACGGAACCCTC	Primer used for quantitative real-time PCR
ME1_R	GATCTCCTGACTGTTGAAGGAAG	Primer used for quantitative real-time PCR
CFD_F	GACACCATCGACCACGACC	Primer used for quantitative real-time PCR
CFD_R	GCCACGTCGCAGAGAGTTC	Primer used for quantitative real-time PCR
IDH3A_F	GGACCTGGAGGAAAGTGGAT	Primer used for quantitative real-time PCR
IDH3A_R	GCTGCTATTGGGGTCTTCAA	Primer used for quantitative real-time PCR
β-actin_F	CATGCCATCCTGCGTCTGGA	Primer used for quantitative real-time PCR
β-actin_R	CCGTGGCCATCTCTTGCTCG	Primer used for quantitative real-time PCR